9-15-2020

Zika Virus Infection Causes Widespread Damage to the Inner Ear

Kathleen T. Yee
University of Mississippi Medical Center

Biswas Neupane
University of Southern Mississippi, biswas.neupane@usm.edu

Fengwei Bai
University of Southern Mississippi, Fengwei.Bai@usm.edu

Douglas E. Vetter
University of Mississippi Medical Center, dvetter@umc.edu

HHS Public Access

Author manuscript

Hear Res. Author manuscript; available in PMC 2021 September 15.

Published in final edited form as:

Hear Res. 2020 September 15; 395: 108000. doi:10.1016/j.heares.2020.108000.

Zika Virus Infection Causes Widespread Damage to the Inner Ear

Kathleen T. Yee[1], **Biswas Neupane**[2], **Fengwei Bai**[2,*], **Douglas E. Vetter**[1,*]

[1]Department of Neurobiology and Anatomical Sciences, University of Mississippi Medical Center, Jackson, MS 39202 USA

[2]Department of Cell and Molecular Biology, University of Southern Mississippi, Hattiesburg, MS 39406, USA

Abstract

Zika virus (ZIKV) has been recently recognized as a causative agent of newborn microcephaly, as well as other neurological consequences. A less well recognized comorbidity of prenatal ZIKV infection is hearing loss, but cases of hearing impairment following adult ZIKV infection have also been recognized. Diminished hearing following prenatal ZIKV infection in a mouse model has been reported, but no cellular consequences were observed. We examined the effects of ZIKV infection on inner ear cellular integrity and expression levels of various proteins important for cochlear function in type I interferon receptor null (*Ifnar1*$^{-/-}$) mice following infection at 5–6 weeks of age. We show that ZIKV antigens are present in cells within the cochlear epithelium, lateral wall, spiral limbus and spiral ganglion. Here we show that ZIKV infection alters cochlear expression of genes that signal cell damage (S100B), transport fluids (AQP1), are gaseous transmitters (eNOs) and modulate immune response (F4/80). Morphological analyses shows that not only are cochlear structures compromised by ZIKV infection, but damage also occurs in vestibular end organs. ZIKV produces a graded distribution of cellular damage in the cochlea, with greatest damage in the apex similar to that reported for cytomegalovirus (CMV) infection. The graded distribution of damage may indicate a differential susceptibility to ZIKV along the cochlear tonotopic axis. Collectively, these data are the first to show the molecular and morphological damage to the inner ear induced by ZIKV infection in adults and suggests multiple mechanisms contributing to the hearing loss reported in the human population.

1. Introduction

Zika virus (ZIKV), first identified in 1947 in a non-human primate in the Zika Forest in Uganda (Dick et al., 1952), was relatively innocuous to humans with low infection rates for over half a century. A significant human health concern has been the escalation of infection

*Corresponding Authors: Fengwei Bai, Ph. D., fengwei.bai@usm.edu; Telephone 601-266-4748; and Douglas E. Vetter. Ph.D., dvetter@umc.edu; Telephone 601-984-1689.

Declaration of competing interest

Nothing to declare.

rates in recent years. In 2013, outbreaks occurred in Micronesia, infecting more than 70% of the population over 3 years of age (Duffy et al., 2009) and in French Polynesia (Cao-Lormeau et al., 2014). In 2015, Central and South American countries and U.S. Territories, including the Virgin Islands and Puerto Rico, reported broad spread of ZIKV infection with correlated incidence of microcephalic births (Brasil et al., 2016; Cuevas et al., 2016; Shapiro-Mendoza et al., 2017). In 2016, investigations of 29 ZIKV infected individuals in southern Florida provided evidence that ZIKV mosquitos were present in the continental United States (Likos et al., 2016). While ZIKV-carrying mosquitos, *Aedes aegypti*, are the primary vector for ZIKV transmission, the geographic distribution of ZIKV infected individuals is broader than the ZIKV-transmitting mosquito habitat. This mismatch is likely due to the fact that ZIKV transmission can also occur between humans, and human world-wide travel enables geographic spread of the virus. (Hills et al., 2016). High ZIKV titers in semen of infected males (Lazear et al., 2016; Mansuy et al., 2016) contributes to spread through sexual contact (Musso et al., 2015b; D'Ortenzio et al., 2016), but it can also spread through saliva (Musso et al., 2015a). ZIKV transmission from an infected mother to her developing fetus (Besnard et al., 2014) can cause developmental defects, including microcephaly (Rasmussen et al., 2016). Perhaps of greater concern is case-study data indicating ZIKV transmission from patient to care-taker in the absence of sexual contact or any other known risk factors (Brent et al., 2016). While micocephaly has garnered the world's attention, much research on ZIKV is still required, including the consequences to organs affected by ZIKV infection beyond the brain.

Mouse models first revealed that ZIKV could infect organs outside of the nervous system (Aliota et al., 2016) before recognition of this occurence in humans (Valdespino-Vazquez et al., 2019). ZIKV injected to the footpad of interferon α/β,-γ receptors (type I and II IFN receptors, AG129) null mice infected the brain plus numerous visceral organs (Aliota et al., 2016). *In utero* transmission of ZIKV to the developing fetus can result in impaired hearing (Leal et al., 2016a; Leal et al., 2016b) and adults infected with ZIKV have reported transient hearing loss (Vinhaes et al., 2017). Hearing impairment modeled in AG129 mice prenatally infected with ZIKV show compromised auditory thresholds without any detectable hair cell loss (Julander et al., 2018). Because varied populations of cochlear cells play critical roles in mechano-transduction and hair cell activation, a relatively large number of targets exist that could explain ZIKV-mediated hearing loss. Since clinical evidence suggests that adult ZIKV infection can result in a loss of hearing, we investigated the effects of postnatal ZIKV infection on structures other than the brain that could explain these clinical results; we studied the structural outcomes of ZIKV infection on the inner ear. We were interested in 1) assessing whether ZIKV administration mimicking normal hematogenous delivery of virus in humans could infect cells in the cochlea; and if so, 2) whether ZIKV infection would result in altered protein expression and anatomical consequences to the inner ear. Immune compromised, interferon α/β receptor null mice (*Ifnar1*$^{-/-}$) were used for postnatal ZIKV infection because wild type mice exhibit a more robust interferon response compared to humans that must be overcome for viral replication (Grant et al., 2016; Lazear et al., 2016; Mounce et al., 2016; Rossi et al., 2016). Secondly, diminished immune signaling is relevant to immune compromised patients who have greater susceptibility to viral infection. We

report here on localized protein expression changes and cellular morphological consequences to the inner ear following postnatal ZIKV infection.

2. Materials and Methods

2.1 Animals and Zika virus

Ifnar1$^{-/-}$ mice (C57BL/6J background) were bred in-house (The University of Southern Mississippi [USM]) and maintained in a 12 hour light-cycle with lights on at 7am and lights off at 7pm. At weaning, mice were group-housed by sex. The Zika virus (ZIKV) strain PRVABC59, closely related to the epidemic strains linked to human microcephaly in the Americas (Faria et al., 2016), was obtained from B. Johnson (CDC Arbovirus Branch, Fort Collins, CO, USA). ZIKV PRVABC59 was propagated in African green monkey kidney epithelial Vero cells (ATCC CCL-81). Viral stocks were titered in Vero cells by a plaque assay according to Paul et al. (Paul et al., 2014).

All animal care and experiments were conducted in accordance with the Guide for the Care and Use of Laboratory Animals approved by the USM IACUC Committee. All ZIKV infections and handling of ZIKV-infected mice were performed by certified personnel in biosafety level 3 laboratories following standard biosafety protocols approved by the USM Institutional Biosafety Committees.

2.2 ZIKV inoculations, controls and survival time

Five to six-week old *Ifnar1*$^{-/-}$ male and female mice were injected either with 1×10^5 PFU of ZIKV in 50μl phosphate-buffered saline (PBS) via foot-pad (n= 14; 7 females and 7 males), or 50μl of PBS only (vehicle control) (n=7; 4 females and 3 males), or were uninjected (n=6; 3 females and 3 males). Mice survived for 9-days post-injection and uninjected mice were age-matched.

2.3 Tissue harvest and preparation; immunohistochemistry and microscopy

Mice were perfused (4% paraformaldehyde or 2.5% glutaraldehyde), temporal bones were isolated and prepared for cryostat (16μm) or ultramicrotome sectioning (3 – 4.5μm). Cryostat sectioned material was immunohistochemically stained with primary antibodies 4G2 purified from hybridoma cell culture (ATCC HB-112), AQP1 and S100b (Santa Cruz Biotechnology, Dallas, TX, USA), Myosin VIIa (Proteus Biosciences, Ramona, CA, USA), F4/80 (Synaptic Systems, Goettingen, Germany) or endothelial nitric oxide synthase (eNOS, Chemicon/Millipore, Sigma, Pittsburgh, PA, USA). Both cochleas from each mouse were analyzed. Immunofluorescence was visualized using confocal microscopy (Nikon C1 Confocal). Glutaraldehyde-fixed tissue was processed for plastic embedding in Araldite and sectioned (3 – 4.5μm) with a rotary ultramicrotome, stained with toluidine blue and imaged with light microscopy (Leitz DMRX) and photographed (Spot Camera). Inner ear images from Araldite-embedded temporal bones were provided for classification as ZIKV-infected or control to two individuals blind to the treatment condition of each case. There was complete agreement between the judgement of the blind reviewers and actual viral treatment condition. In all analyses presented, no difference was observed between sexes or between vehicle-injected mice and uninjected mice.

3. Results

3.1 ZIKV antigen can be detected in the inner ear /cochlea

To examine if ZIKV targets the inner ear, we infected *Ifnar1*$^{-/-}$ mice, which are deficient in receptors of type I (α/β) interferon, with ZIKV via a footpad inoculation route at 5–6 weeks of age. Based on previous studies showing *in vivo* ZIKV cellular infection occurs between five (Uraki et al., 2017; Tan et al., 2018) and 14 days (Clancy et al., 2019) following ZIKV administration, we chose an intermediate survival time of 9-days post-injection. The expectation was that following a 9-day survival, ZIKV-infected cells would be detectable, yet the intermediate survival time would also be sufficient for any cellular changes to occur. On day 9 post-infection, immunohistochemistry was performed with 4G2, an antibody specific to flavivirus E protein (Conte et al., 2017), to detect ZIKV envelope (E) protein antigens in cells of the cochlea. The immunostaining showed that ZIKV E was readily detected in the cochlear epithelium, including support cells of the inner sulcus of the spiral limbus (medial support cells, Figure 1A”, D’, D”) and support cells lateral to the outer hair cells (OHCs, lateral support cells, Figure 1A”), cells of the spiral limbus (Figure 1B”, B”’), Deiter’s cells (Figure 1A”, C”, D’, D”), inner and outer pillar cells (Figure 1A”, D’, D”) and hair cells (Figure 1D’, D”). Staining of cochlear sections with antibodies to 4G2 and myosin VIIa, a hair cell marker, showed protein co-localization (Figure 1D”), indicating that ZIKV can infect the cochlear sensory hair cells which are critical for normal hearing. 4G2 staining of vehicle injected (control) mice showed no staining in the cochlear epithelium or spiral limbus (Figure 1A–C, A’–C’). In addition, spiral ganglion neurons (SGNs, Figure 2A”, A”’), spiral ganglion axons (Figure 2B”, B”’) and the auditory nerve within the modiolus (Figure 2C”, C”’), were all 4G2 positive at 9 days following ZIKV infection. Vehicle controls showed no staining in SGNs, their spiral ganglion neuron fibers traveling towards the cochlea nor the auditory nerve (Figure 2A–C, A’–C’).

4G2 immunostaining of the cochlear lateral wall also revealed ZIKV infection. Suprastrial and type I fibrocytes (Figure 3A”, A”’) and the stria vascularis (Figure 3A”–D”, A”’–D”’) were all immunoreactive for 4G2. In the stria vascularis, 4G2 immunolabeled cells were located throughout the 3 laminae. In contrast, the 4G2 ZIKV E antigen was not detected in the lateral wall of vehicle-treated or uninjected mice.

3.2 Changes in protein expression in the inner ear following postnatal ZIKV infection in Ifnar1$^{-/-}$ mice

The process of normal hearing depends not only on sensory hair cells but also cells in the lateral wall, including cells of the stria vascularis and the connective tissue cells (fibrocytes) that make up the spiral ligament. Fibrocytes of the spiral ligament are neurochemically heterogeneous and have been classified based on their spatial location and expression of ion transporters (Spicer and Schulte, 1991). Loss of a subpopulation of spiral ligament fibrocytes occurs prior to loss of hair cells or spiral ganglion neurons and correlates with lower hearing thresholds (Hequembourg and Liberman, 2001), supporting the importance of these cells for normal hearing. Within the stria vascularis is an intrastrial fluid-blood barrier comprised of a network of capillaries lined by endothelial cells connected via tight junctions (Juhn, 1988). Cells forming the stria vascularis are critical for maintaining the ionic balance

within the endolymph and perilymph. Previous work has shown that the stria vascularis is susceptible to degeneration caused by CMV infection (Carraro et al., 2017). We show protein expression changes within the lateral wall, both the stria vascularis and the spiral ligament, as well as the epithelium of the cochlea following ZIKV administration by footpad injection.

3.2.1 S100B—S100B, a member of the multifunctional S100 family. S100 family member proteins are low molecular weight calcium-binding proteins with both intracellular and extracellular functions (Donato, 2001; Marenholz et al., 2004). S100 proteins have a role in normal cells as well as in disease states including cancers, inflammatory disorders, psoriasis and cardiomyopathies (Marenholz et al., 2004; Basnet et al., 2019). There are numerous putative roles for the S100 family of proteins, including cell proliferation, differentiation, protein phosphorylation and Ca^{2+} homeostasis (Donato, 2001). S100 is localized within subdomains of the spiral ligament in rodents (Igarashi et al., 1991; Foster et al., 1994) and in humans (Shi et al., 1992). S100B is expressed by glia and released following injury (Rothermundt et al., 2003; Steiner et al., 2008). Altered S100B expression has been associated with neurodegenerative diseases such as Alzheimer's Disease, multiple sclerosis and traumatic brain injury (see reviews (Marenholz et al., 2004; Michetti et al., 2019). S100B expression levels are tightly regulated. At low levels (nanomolar), extracellular S100B mediates neuron growth and survival, while increased concentrations, in the micromolar range, causes apoptosis (Huttunen et al., 2000). *Ifnar1*$^{-/-}$ mice postnatally-infected with ZIKV and examined at post-infection day 9 showed S100B immunoreactivity upregulated in a broader spatial pattern of protein localization in the spiral limbus and the cochlear epithelium (Figure 4E, F) compared to vehicle controls. Notable is the protein expression in the medial and lateral support cells (Figure 4E, F). In the lateral wall, S100B upregulation occurred in the stria vascularis (Figure 4G, H). Based on the location of the immunoreactivity, putative cells impacted may be cells in the intermediate layer of the stria vascularis or cells of the vascular network. In mice injected with vehicle, the spiral limbus shows S100B localization in a small region medially, but there is no S100B staining of the cochlear epithelium (Figure 4A, B) nor of the stria vascularis (Figure 4C, D). Interestingly, S100B immunoreactivity was detected on the underside of the tectorial membrane (Figure 4E, F) and may reflect extracellular release of S100B and subsequent binding to the tectorial membrane. The lack of immunoreactivity within the entire tectorial membrane suggests this staining pattern is not the result of non-specific binding of antibody typically seen in the tectorial membrane.

3.2.2 Aquaporin-1 (AQP1)—A water channel protein, first identified in the membranes of erythrocytes (Benga et al., 1986b; Benga et al., 1986a) and later named AQP1, is expressed broadly in the body (Nielsen et al., 1993; Effros et al., 1997; Devuyst et al., 1998). AQP1 expressing cells are involved in secretion and absorption processes (Nielsen et al., 1993). AQP1 is among the many AQP family members expressed in the inner ear (Eckhard et al., 2012). Studies have reported varied sites of expression within the inner ear, with notable species differences (Miyabe et al., 2002), but consensus exists amongst studies on the expression of AQP1 in type III fibrocytes of the spiral ligament in guinea pigs, (Stankovic et al., 1995), rodents (Miyabe et al., 2002; O'Malley et al., 2009; Takumida et al.,

2012) and humans (Lopez et al., 2007). In ZIKV injected *Ifnar1*$^{-/-}$ mice, strong AQP1 localization was seen in the middle laminae of the stria vascularis (Figure 5C, D) whereas it was absent under vehicle injected cases (Figure 5A, B). ZIKV injected *Ifnar1*$^{-/-}$ mice showed upregulation of AQP1 localization in type 1 and suprastrial fibrocytes (Figure 5C, D), but not in vehicle-injected mice (Figure 5A, B). AQP1 was upregulated in ZIKV-infected mice and seen outlining vascular-like structures in the osseous spiral lamina above the scala vestibuli (Figure 5C, D) compared to lower expression in vehicle-treated mice (Figure 5A, B). In both vehicle and infected cases (Figure 5C, D), AQP-1 localization within the lateral wall mirrored previous reports showing antibody staining in type III fibrocytes of the spiral ligament and a paucity of AQP1 throughout the remainder of the lateral wall. Significantly, nine days following ZIKV infection of 5–6 week old *Ifnar1*$^{-/-}$ mice, clusters of unattached (floating) AQP1-positive, DAPI-coincident cells were observed within the scala media (Figure 5C, D).

Given that the stria vascularis is targeted by CMV (Carraro et al., 2017), that it plays an important role in regulating the endolymphatic ionic balance required for hearing, and that ZIKV infection produced an upregulation of protein expression within the stria vascularis (including within putative blood vessels), we investigated whether ZIKV infection affects expression of the vascular regulator, endothelial nitric oxide synthase.

3.2.3 Endothelial nitric oxide synthase (eNOS)—eNOS belongs to a family of enzymes that catalyzes L-arginine to nitric oxide and functions as a cellular signaling molecule. Nitric oxide is a gaseous transmitter involved in normal physiological processes throughout the body (Pacher et al., 2007), including the cochlea (Popa et al., 2001; Takumida and Anniko, 2001b, a, 2002, 2004). Endothelial nitric oxide synthase (eNOS) is well recognized as a regulator of vascular tone and is also expressed in the cochlear epithelium (Heinrich et al., 2005), the stria vascularis and spiral ligament (Yamane et al., 1997; Liu et al., 2008). Nitric oxide has a role in signal transduction and ion regulation in the cochlea. Changes in NO concentration can affect cellular processes that lead to protection or cell death (Pacher et al., 2007). Following pneumococcal meningitis infection, which disrupts the inner ear blood-labyrinth barrier, eNOS is upregulated in spiral ligament blood vessels, the stria vascularis and spiral ganglion blood vessels (Kastenbauer et al., 2001).

In *Ifnar1*$^{-/-}$ vehicle-treated mice, a baseline level of eNOS was detected in the stria vascularis as fine, diffuse immunoreactivity (Figure 6E, F). eNOS was also detected within the spiral ligament, predominantly in type I and type III fibrocytes (Figure 6A, B, E, F). Vehicle-treatment also showed baseline expression of eNOS in the spiral ganglion and auditory nerve (Figure 6I and K).

Nine days following ZIKV infection of 5–6-week-old *Ifnar1*$^{-/-}$ mice, eNOS immunoreactivity appeared as less diffuse, larger aggregates in the stria vascularis (Figure 6C, D, G, H), suggesting an upregulation over baseline. Immunoreactivity for eNOS was also upregulated in the spiral ligament (Figure 6C, D, G, H) in type I, II, III, and suprastrial fibrocytes. In the modiolus, eNOS protein expression was upregulated in the region of the

spiral ganglion with prominent immunoreactivity in extra-neuronal structures and in the auditory nerve (Figure 6J, L).

3.2.4 F4/80—S100 protein family members signal signs of danger / trauma and S100B signaling acts on macrophages and biases their function towards an inflammatory response (Okuda et al., 2012). S100B acts as a chemokine; its overexpression and release from glial tumors causes chemoattraction of macrophages toward the tumor contributing to an increase in tumor size (Wang et al., 2013). Since our data indicate that S100B protein expression levels increase following ZIKV infection, we assessed whether a concomitant increase in the macrophage population occurs in the cochlea. The protein F4/80, also known as EGF-like module-containing mucin-like hormone receptor-like 1 (EMR1), is expressed by mature macrophages. We used an antibody against F4/80 to stain the inner ear of postnatally ZIKV infected or vehicle injected *Ifnar1*$^{-/-}$ mice to assess macrophage marker expression in the cochlea. No detectable F4/80 was observed in the cochlear epithelium (Figure 7A and B) of *Ifnar1*$^{-/-}$ vehicle-treated mice. However, in ZIKV-infected *Ifnar1*$^{-/-}$ mice, F4/80 was upregulated in the cochlear epithelium (Figure 7C, D) and in cells beneath the basilar membrane (Figure 7C, D, E, G), positioned in a regional cochlear macrophage niche (Hirose et al., 2005; Lang et al., 2006; Tornabene et al., 2006; Okano et al., 2008; Sato et al., 2008; Yang et al., 2015).

3.3 Cellular consequences of ZIKV infection

Based on the protein expression changes in the cochlear epithelium and the lateral wall, we were interested in assessing the structural state of the inner ear following ZIKV infection.

3.3.1 Structural cochlear damage induced by postnatal ZIKV infection of Ifnar1$^{-/-}$ mice—The cochlear epithelium of *Ifnar1*$^{-/-}$ vehicle-injected mice exhibited the expected anatomical organization (Figure 8A and B). Inner and outer pillar cells border the sides of the tunnel of Corti. Positioned toward the modiolus are the inner hair cell and medial support cells and located laterally are the outer hair cells and lateral support cells. In contrast, the epithelium of the cochlea isolated from ZIKV-infected mice exhibited significant aberrant organization (Figure 8G, H, K, L). Many cells within the cochlear epithelium appeared swollen (Figure 8G, H, K, L). The epithelium of the middle cochlear turn, while clearly abnormal, still maintained recognizable cellular organization that resembled the normal epithelium (Figure ZIKV-infected, 8H to vehicle injected, 8B). However, the epithelium of the apical turn contained greater damage and disorganization (Figure 8K, L) than the other turns. The nuclei of medial support cells were displaced from the basal aspect of the cells (vehicle injected, Figure 8B to ZIKV-infected, Figure 8H, L). Myelinated axons and dendrites located beneath the spiral limbus of vehicle-treated mice had slender, compact profiles (Figure 8C), but in ZIKV-infected mice, the axons and dendrites were enlarged and had a swollen, watery appearance (Figure 8I, M). The spiral limbus of vehicle-injected mice showed normal integrity (Figure 8A, D), but vacuolation of the spiral limbus and disruption of its surface was observed in ZIKV-infected mice, potentially due to spiral limbus fibrocyte damage at the level of the middle turn (Figure 8G, J). The vacuolation and surface cavitation of the spiral limbus was most severe at the apex (Figure 8K, N).

The stria vascularis and spiral ligament integrity were normal in *Ifnar1*$^{-/-}$ vehicle-treated mice (Figure 8E, F). ZIKV-infection produced damage in both the stria vascularis and the spiral ligament (Figure 8O, P, Q, R). Many spiral ligament fibrocytes appeared to lack cytoplasm and presented with a vacuolated appearance (Figure 8O and P). Some regions of the lateral wall showed a loss of continuity between the stria vascularis and spiral ligament (Figure 8G, K, O, and P) suggestive of localized edema. Additionally, the apical surface of the stria vascularis was also seen in certain regions to form protrusions of cytoplasm containing vesicles or vacuoles (Figure 8O). Evidence of release of vessicles was observed and in some cases translocation of the nucleus to the apical surface was observed, possibly suggesting imminent expulsion of the cell from the epithelium (Figure 8O, P, Q, R).

Since our data on the cochlear epithelium, spiral limbus and fibers beneath the spiral limbus clearly showed a differential effect of ZIKV infection along the tonotopic axis of the cochlea (worst at the apical low frequency region versus less damage in the mid-frequency middle turn), and since it has previously been shown that CMV infection also produces greater damage in apical regions (Carraro et al., 2016; Carraro et al., 2017), we sought to determine whether the morphology of spiral ganglion neurons (SGN) might also differ at the apical, middle and basal turns along the cochlear spiral. At all three levels of the cochlea, vehicle-injected mice exhibited SGNs with normal neuronal morphology, well-defined nuclei, prominent nucleoli and uniformly stained cytoplasm (Figure 9A–C). The SGNs were also surrounded by small diameter axon profiles that are tightly compact. In contrast, it was qualitatively evident that the axon profiles in ZIKV-treated mice were larger (Figure 9D–F) compared to vehicle-treated mice (Figure 9A–C). The SGNs in ZIKV-infected mice were also dramatically altered (Figure 9D–F). Many SGNs in the apical aspect of the cochlea contained a patchy or mottled cytoplasm in which vacuoles could be seen. Some cell profiles showed greatly reduced cytoplasmic contents while others appeared to be nearly devoid of cytoplasm. A nuclear profile similar to the apical SGNs in vehicle-treated mice could not be discerned in the same cochlear region in ZIKV-infected mice. The ZIKV-infected apical SGN nuclei appeared to be smaller in size with more heterochromatic (condensed) DNA (Figure 9D). At the level of the middle turn, the nuclei in SGN of ZIKV infected mice were more condensed than in vehicle-treated cases (cf. Figure 9E to Figure 9B), but their cell bodies appeared less swollen and their cytoplasm, while still mottled, more completely filled the cell. In the base of the cochlea, some cells showed lightly-stained, mottled cytoplasm, but many others exhibited a more uniformly-stained cytoplasm (Figure 9F). While ZIKV-infected basal SGNs had a more normal appearance to their cytoplasm than the apical SGNs, the SGN soma were enlarged compared to vehicle-treated cases (cf. Figure 9F to 9C).

3.3.2 Vestibular cellular morphological analysis of ZIKV-infected Ifnar1$^{-/-}$ mice—

Given the morphological changes to structure of the cochlea induced by ZIKV infection, we questioned whether damage to the inner ear following ZIKV infection was restricted to the cochlea, or whether it could also impact vestibular end organs.

3.3.2.1 Saccular macula: The saccular macula, one of the maculae that detects linear acceleration (Lowenstein, 1952), was assessed for morphological changes following ZIKV infection. In *Ifnar1*$^{-/-}$ vehicle-treated mice, the saccular macula was well-stained and

contained closely-packed epithelium of normal morphology (Figure 10A and B). Some of the flask-shaped hair cells were seen to be in continuity with stereocilia at the apical surface (Figure 10B). Otoconia were visible above the saccular macula (Figure 10B). In *Ifnar1*$^{-/-}$ mice infected with ZIKV, the epithelium of the saccular macula contained many cellular vacuoles that in some instances included cellular remnants (Figure 10C, D). Some of the vacuoles were presumed to have been occupied by hair cells based on their continuity with the apical surface (Figure 10D). Nuclei were seen in the endolymph above the epithelium of the saccular macula (Figure 10D) and may have been extruded from the epithelium as nuclei located at the epithelial surface of the saccular macula could be seen that were likely in the process of extrusion (Figure 10D).

3.3.2.2 Posterior canal crista ampullaris: The canal cristae allow for the detection of angular acceleration/rotation (Lowenstein, 1952). In *Ifnar1*$^{-/-}$ vehicle-treated mice, as with the saccular macula, the posterior canal crista was normal in appearance; hair cells were closely juxtaposed to neighboring support cells and were seen to extend stereocilia above the apical epithelial surface (Figure 11A and B). In *Ifnar1*$^{-/-}$ mice infected with ZIKV, the epithelium of the crista ampullaris of the posterior canal (Figure 11D) was vacuolated. Cell remnants were observed in some of the vacuolar spaces (Figure 11E). The axons innervating the posterior canal crista appeared qualitatively larger in diameter (Figure 11D) compared to vehicle-treated vestibular axons (Figure 11A). An example of a nucleus positioned at the apical surface, possibly in the process of extrusion (Figure 11E) could be seen. Vesicles could be seen in the endolymph above the epithelium of the crista ampullaris, suggestive of an ongoing process of exocytosis from the epithelium (Figure 11G and I). Due to the critical role of the crista ampullaris in the maintenance of balance, unilateral vestibular end organ damage can cause difficulty with locomotion. However, damage to the posterior canal crista was bilateral in nature (cf. Figure 11G, H). Large vacuoles, only evident in ZIKV-infected epithelium of the crista ampullaris, were seen within the epithelium of the posterior canal crista of both inner ears (Figure 11G, H). Located in the semicircular canal epithelium positioned lateral to the base of the crista ampullaris are the dark cells which function in a manner similar to the stria vascularis and are also critical for K^+ regulation of the local endolymph. In vehicle-treated mice, dark cells at the base of the crista ampullaris exhibited normal morphology; dark cell nuclei were located apical to basal infoldings/striations (Figure 11C, C'). In contrast, epithelium in a comparable region in ZIKV-infected mice showed copious vacuoles nearly completely filling the cells of the epithelium (Figure 11F and inset F') to the extent that the striations beneath the dark cell nuclei were no longer visible.

4. Discussion

4.1 Viral delivery route and cellular consequences

Viral infection studies have primarily used two approaches: 1) direct viral exposure to the region of interest, or 2) systemic administration at a distance allowing for a hematogenous route of infection. The infectability of the inner ear and its cell types varies depending on route of viral inoculation. The same strain of guinea pig cytomegalovirus (GPCMV) injected intracardially (Fukuda et al., 1988) and intracochlearly (Keithley et al., 1988) yielded

drastically varied patterns of damage. Direct scala tympani GPCMV inoculation showed degeneration of the organ of Corti, the stria vascularis, swelling of spiral ganglion axons and robust macrophage infiltration in the scala tympani that expanded over time to include the scala vestibuli and the modiolus and spiral ligament. In contrast, GPCMV injected into the heart, at even higher doses, showed hematogenous infection only of spiral ganglion neurons and blood vessels within the modiolus.

The method of inoculation by foot pad injection was utilized to mimic the hematogenous route of ZIKV inoculation in humans occurring through mosquitos or other humans. We reasoned that consequences of ZIKV infection conducted in this manner would also more accurately parallel changes in protein expression and cellular damage seen in humans when the viral inoculation site is distant from the organ of interest.

4.2 Potential for strial blood-endolymph membranous labyrinth damage

Changes in protein localization and alterations in cellular morphology in the stria vascularis following ZIKV infection are suggestive that ZIKV infection compromises the blood-endolymph membranous labyrinth barrier. Upregulation of S100B, a Damage-Associated Molecular Pattern Molecule (DAMP) is suggestive of trauma. AQP1, a water channel, supports greater fluid flux in the intermediate region of the stria vascularis, in a pattern that is resembles labeled blood vessels in the stria. eNOS expression upregulated more broadly within the stria vascularis are indicative of cellular changes in this region following Zika virus infection. It is possible that elevated levels of S100B may provide a signal that result in changes in AQP1 and eNOS protein expression. Cytomegalovirus infection of the cochlea following intracerebral virus injection revealed permeability of the blood-labyrinth barrier (Li et al., 2014).

Following ZIKV infection, vesicles and vacuoles form and nuclei are seen to move from the stria vascularis into the endolymph likely as by-products of cellular damage from excess load on the system. The stria vascularis is essential for production of endolymph, a fluid high in potassium, low in sodium, producing an endocochlear potential of +80mV compared to perilymph (Von Bekesy, 1952). Gene deletion of molecules expressed within the stria vascularis disrupts the endocochlear potential, impairs hearing (Gow et al., 2004; Kitajiri et al., 2004; Cohen-Salmon et al., 2007), and can result in cell death within both the cochlea and vestibular end organs (Vetter et al., 1996). Through potassium transporter expression in fibrocytes, the spiral ligament also contributes to producing the endocochlear potential (Schulte and Adams, 1989; Schulte and Steel, 1994; Crouch et al., 1997; Sakaguchi et al., 1998). Gap junctions feature prominently in the lateral wall and connect spiral ligament fibrocytes and basal and intermediate cells of the stria vascularis, forming a functional syncytium (Forge, 1984; Kikuchi et al., 1995; Xia et al., 1999; Xia et al., 2000; Xia et al., 2001). Expressed in the stria vascularis and spiral ligament during development (Xia et al., 1999) and spiral ligament at maturity is *GJB2* (connexin 26); when mutated (Xia et al., 1998), ion recycling in the cochlea and endolymph ionic balance are both compromised and deafness ensues (Xia et al., 1998). Cellular phenotypes in ZIKV infected mice showing altered morphologies in the stria vascularis and spiral ligament and disruption of their normal close juxtaposition likely represent a significant anatomical substrate for

compromised hearing in these mice. In cochlear otosclerosis, spiral ligament damage from cochlear endosteum invasion with fibrous overgrowth and altered blood supply results in stria vascularis atrophy that correlates with hearing loss measured via pure-tone averages of bone-conduction hearing thresholds (Doherty and Linthicum, 2004).

4.3 Cochlear macrophage expression following viral infection

Similar to our findings of SGN damage and macrophage presence in a well-described niche beneath the basilar membrane (Hirose et al., 2005; Lang et al., 2006; Tornabene et al., 2006; Okano et al., 2008; Sato et al., 2008; Yang et al., 2015), cytomegalovirus injected into the cerebral hemisphere of neonatal mice infects spiral ganglion neurons, increases in the macrophage population that produces and upregulates reactive oxygen species and induces sensorineural hearing loss (Schachtele et al., 2011). The upregulation of macrophages observed following ZIKV infection may also increase reactive oxygen species production that contributes to damage in the inner ear. Ablation of a macrophage inflammatory protein was protective against hearing loss in guinea pigs compared to wild type cohorts (Schraff et al., 2007).

4.4 ZIKV infection in relation to cumulative cellular damage

We show that following ZIKV infection, a subset of cochlear cells are immunolabeled with 4G2 antibody against the ZIKV envelope E protein. Yet, the ZIKV infected cells are spatially more restricted than the cumulative cellular damage seen locally, for example in the lateral wall. A possible explanation for these seemingly disparate findings is that some cells may have previously been infected and already cleared the viruses by 9 days post-infection and no longer harbor detectable ZIKV envelope proteins by 4G2 immunostaining. Thus, the 4G2 distribution detected at 9 day post-infection may represent the entirety of 4G2-positive cells at this time point. A viral infection limited in the number of cells affected could nonetheless produce more wide-spread cumulative cellular damage locally via by gap junctions that connect cells of the spiral ligament and the stria vascularis, for example. The normal role of the lateral wall to maintain ionic balance may also allow for the spread of damage-associated signaling more broadly beyond the directly infected cells following ZIKV infection.

The presence of a dimishing apical to basal gradient of damage in the cochlear epithelium, spiral limbus, spiral ganglion neurons and their axons and fibers supports the idea that the cochlea is differentially affected by ZIKV infection. The graded distribution of damage with the apex most strongly affected is particularly intriguing since damage often initially manifests in the base of the cochlea following other viral infections [measles (Lindsay and Hemenway, 1954) mumps (Lindsay et al., 1960)] and noise exposure (Wang and Ren, 2012; Jensen et al., 2015). These mirror the normal involvement of the base in aging (Hequembourg and Liberman, 2001). It is currently not known whether the apex of the cochlea is more susceptible to direct ZIKV infection or whether the damage induced by ZIKV manifests more strongly in the apex, which needs further investigation.

4.5 ZIKV-induced vestibular damage

Substantial cumulative cellular damage occurs in vestibular end organs mediating rotation and linear acceleration following ZIKV infection. Patients infected with ZIKV have not reported vestibular difficulties or problems with balance, but interestingly, 3-week-old type I and type II IFN null mice (AG129) 6 days post-ZIKV infection exhibited a loss of balance along with other neurological disease phenotypes (Rossi et al., 2016). Perhaps, ZIKV-induced vestibular end organ damage may have an asymmetric onset that later results in bilateral damage. If the initial damage is asymmetric, patients might not specifically sense any vestibular problems due to overall malaise from symptoms of ZIKV infection.

Both the sensory epithelium of the cochlea and vestibular system along with their associated epithelia, the stria vascularis and dark cell epithelium, respectively, all show damage following ZIKV infection. Damage to the sensory epithelia provides anatomical evidence for a direct and non-recoverable impact on hearing. The stria vascularis of the cochlea and the dark cell epithelium of the utricle and ampullae are morphologically similar (Kimura, 1969), each of which contributes to maintaining high K^+ in the endolymph. Marginal cells of the stria vascularis and dark cells of the vestibular system both transport K^+ from their basal surface out through the apical aspect of the cell (Marcus and Shen, 1994; Marcus and Shipley, 1994). ZIKV-infection alters the morphology of the stria vascularis cells and dark cells in the dark cell epithlelium, producing vacuoles and disorganization and reduction of basal striations necessary for ion flux, likely compromising endolymph production in both of these regions. The extent to which this may represent transient disruptions to hearing and balance remains unknown.

This data demonstrates for the first time that hematogenously transported ZIKV infects the cochlea and induces significant cellular damage to many regions of the cochlea and all vestibular end organ types. Cumulatively, damage to these regions of the cochlea are highly suggestive of ZIKV-induced hearing loss. Functional loss has been verified in other studies (Julander et al., 2018). Unfortunately, use of live animals infected with ZIKV is not yet possible at all Institutions, thus precluding hearing assays in this study. Finally, ZIKV infection alters expression of various cochlear proteins known to be involved in injury, fluid flux, and cell signaling. These data suggest possible mechanisms that may underlie the reports of hearing dysfunction in humans following ZIKV infection at adulthood and suggest clinical audiometric testing should be performed on suspected adult-stage ZIKV patients. Further, it is imperative to understand the sites of damage occurring to the inner ear following ZIKV infection so that future therapies can be intelligently designed to mitigate hearing impairment associated with ZIKV infection.

Funding

Supported in part by: NIH R15AI135893 (F.B.), NIH R21DC015124 (D.E.V.), UMMC Intramural Research Support Program (D.E.V and K.T.Y.), UMMC Excellence in Research Award (D.E.V.). Confocal imaging supported by the Center for Psychiatric Neuroscience Imaging Core, COBRE P30 GM103328. None of the funding sources had any influence on this study.

ABBREVIATED TITLE:

ZIKV Infection Causes Inner Ear Damage

References

Aliota MT, Caine EA, Walker EC, Larkin KE, Camacho E, Osorio JE (2016) Characterization of Lethal Zika Virus Infection in AG129 Mice. PLoS Negl Trop Dis 10:e0004682. [PubMed: 27093158]

Basnet S, Sharma S, Costea DE, Sapkota D (2019) Expression profile and functional role of S100A14 in human cancer. Oncotarget 10:2996–3012. [PubMed: 31105881]

Benga G, Popescu O, Pop VI, Holmes RP (1986a) p-(Chloromercuri)benzenesulfonate binding by membrane proteins and the inhibition of water transport in human erythrocytes. Biochemistry 25:1535–1538. [PubMed: 3011064]

Benga G, Popescu O, Borza V, Pop VI, Muresan A, Mocsy I, Brain A, Wrigglesworth JM (1986b) Water permeability in human erythrocytes: identification of membrane proteins involved in water transport. Eur J Cell Biol 41:252–262. [PubMed: 3019699]

Besnard M, Lastere S, Teissier A, Cao-Lormeau V, Musso D (2014) Evidence of perinatal transmission of Zika virus, French Polynesia, December 2013 and February 2014. Euro Surveill 19.

Brasil P et al. (2016) Zika Virus Infection in Pregnant Women in Rio de Janeiro. The New England journal of medicine 375:2321–2334. [PubMed: 26943629]

Brent C, Dunn A, Savage H, Faraji A, Rubin M, Risk I, Garcia W, Cortese M, Novosad S, Krow-Lucal ER, Crain J, Hill M, Atkinson A, Peterson D, Christensen K, Dimond M, Staples JE, Nakashima A (2016) Preliminary Findings from an Investigation of Zika Virus Infection in a Patient with No Known Risk Factors - Utah, 2016. MMWR Morb Mortal Wkly Rep 65:981–982. [PubMed: 27631467]

Cao-Lormeau VM, Roche C, Teissier A, Robin E, Berry AL, Mallet HP, Sall AA, Musso D (2014) Zika virus, French polynesia, South pacific, 2013. Emerg Infect Dis 20:1085–1086. [PubMed: 24856001]

Carraro M, Park AH, Harrison RV (2016) Partial corrosion casting to assess cochlear vasculature in mouse models of presbycusis and CMV infection. Hearing research 332:95–103. [PubMed: 26707615]

Carraro M, Almishaal A, Hillas E, Firpo M, Park A, Harrison RV (2017) Cytomegalovirus (CMV) Infection Causes Degeneration of Cochlear Vasculature and Hearing Loss in a Mouse Model. J Assoc Res Otolaryngol 18:263–273. [PubMed: 27995350]

Clancy CS, Van Wettere AJ, Morrey JD, Julander JG (2019) Zika Virus Associated Pathology and Antigen Presence in the Testicle in the Absence of Sexual Transmission During Subacute to Chronic Infection in a Mouse Model. Scientific reports 9:8325. [PubMed: 31171800]

Cohen-Salmon M, Regnault B, Cayet N, Caille D, Demuth K, Hardelin JP, Janel N, Meda P, Petit C (2007) Connexin30 deficiency causes instrastrial fluid-blood barrier disruption within the cochlear stria vascularis. Proc Natl Acad Sci U S A 104:6229–6234. [PubMed: 17400755]

Conte FP, Martins RS, Cajaraville A, Nascimento HJ, Jurgilas PB, de Lima SMB, Missailidis S, Arissawa M (2017) Production of Monoclonal Antibody That Recognizes Zika Virus and Other Flaviviruses in Serum-Free Conditions. Monoclon Antib Immunodiagn Immunother 36:264–271. [PubMed: 29211630]

Crouch JJ, Sakaguchi N, Lytle C, Schulte BA (1997) Immunohistochemical localization of the Na-K-Cl co-transporter (NKCC1) in the gerbil inner ear. J Histochem Cytochem 45:773–778. [PubMed: 9199662]

Cuevas EL et al. (2016) Preliminary Report of Microcephaly Potentially Associated with Zika Virus Infection During Pregnancy - Colombia, January-November 2016. MMWR Morb Mortal Wkly Rep 65:1409–1413. [PubMed: 27977645]

D'Ortenzio E, Matheron S, Yazdanpanah Y, de Lamballerie X, Hubert B, Piorkowski G, Maquart M, Descamps D, Damond F, Leparc-Goffart I (2016) Evidence of Sexual Transmission of Zika Virus. The New England journal of medicine 374:2195–2198. [PubMed: 27074370]

Devuyst O, Nielsen S, Cosyns JP, Smith BL, Agre P, Squifflet JP, Pouthier D, Goffin E (1998) Aquaporin-1 and endothelial nitric oxide synthase expression in capillary endothelia of human peritoneum. Am J Physiol 275:H234–242. [PubMed: 9688919]

Dick GW, Kitchen SF, Haddow AJ (1952) Zika virus. I. Isolations and serological specificity. Trans R Soc Trop Med Hyg 46:509–520. [PubMed: 12995440]

Doherty JK, Linthicum FH Jr. (2004) Spiral ligament and stria vascularis changes in cochlear otosclerosis: effect on hearing level. Otol Neurotol 25:457–464. [PubMed: 15241221]

Donato R (2001) S100: a multigenic family of calcium-modulated proteins of the EF-hand type with intracellular and extracellular functional roles. Int J Biochem Cell Biol 33:637–668. [PubMed: 11390274]

Duffy MR, Chen TH, Hancock WT, Powers AM, Kool JL, Lanciotti RS, Pretrick M, Marfel M, Holzbauer S, Dubray C, Guillaumot L, Griggs A, Bel M, Lambert AJ, Laven J, Kosoy O, Panella A, Biggerstaff BJ, Fischer M, Hayes EB (2009) Zika virus outbreak on Yap Island, Federated States of Micronesia. The New England journal of medicine 360:2536–2543. [PubMed: 19516034]

Eckhard A, Gleiser C, Arnold H, Rask-Andersen H, Kumagami H, Muller M, Hirt B, Lowenheim H (2012) Water channel proteins in the inner ear and their link to hearing impairment and deafness. Molecular aspects of medicine 33:612–637. [PubMed: 22732097]

Effros RM, Darin C, Jacobs ER, Rogers RA, Krenz G, Schneeberger EE (1997) Water transport and the distribution of aquaporin-1 in pulmonary air spaces. J Appl Physiol (1985) 83:1002–1016. [PubMed: 9292489]

Faria NR et al. (2016) Zika virus in the Americas: Early epidemiological and genetic findings. Science 352:345–349. [PubMed: 27013429]

Forge A (1984) Gap junctions in the stria vascularis and effects of ethacrynic acid. Hearing research 13:189–200. [PubMed: 6715265]

Foster J, Drescher M, Hatfield J, Drescher D (1994) Immunohistochemical localization of S-100 protein in auditory and vestibular end organs of the mouse and hamster. Hearing research 74:67–76. [PubMed: 8040100]

Fukuda S, Keithley EM, Harris JP (1988) Experimental cytomegalovirus infection: viremic spread to the inner ear. Am J Otolaryngol 9:135–141. [PubMed: 2845828]

Gow A, Davies C, Southwood CM, Frolenkov G, Chrustowski M, Ng L, Yamauchi D, Marcus DC, Kachar B (2004) Deafness in Claudin 11-null mice reveals the critical contribution of basal cell tight junctions to stria vascularis function. J Neurosci 24:7051–7062. [PubMed: 15306639]

Grant A, Ponia SS, Tripathi S, Balasubramaniam V, Miorin L, Sourisseau M, Schwarz MC, Sanchez-Seco MP, Evans MJ, Best SM, Garcia-Sastre A (2016) Zika Virus Targets Human STAT2 to Inhibit Type I Interferon Signaling. Cell Host Microbe 19:882–890. [PubMed: 27212660]

Heinrich UR, Selivanova O, Feltens R, Brieger J, Mann W (2005) Endothelial nitric oxide synthase upregulation in the guinea pig organ of Corti after acute noise trauma. Brain Res 1047:85–96. [PubMed: 15890317]

Hequembourg S, Liberman MC (2001) Spiral ligament pathology: a major aspect of age-related cochlear degeneration in C57BL/6 mice. J Assoc Res Otolaryngol 2:118–129. [PubMed: 11550522]

Hills SL, Russell K, Hennessey M, Williams C, Oster AM, Fischer M, Mead P (2016) Transmission of Zika Virus Through Sexual Contact with Travelers to Areas of Ongoing Transmission - Continental United States, 2016. MMWR Morb Mortal Wkly Rep 65:215–216. [PubMed: 26937739]

Hirose K, Discolo CM, Keasler JR, Ransohoff R (2005) Mononuclear phagocytes migrate into the murine cochlea after acoustic trauma. The Journal of comparative neurology 489:180–194. [PubMed: 15983998]

Huttunen HJ, Kuja-Panula J, Sorci G, Agneletti AL, Donato R, Rauvala H (2000) Coregulation of neurite outgrowth and cell survival by amphoterin and S100 proteins through receptor for advanced glycation end products (RAGE) activation. J Biol Chem 275:40096–40105. [PubMed: 11007787]

Igarashi S, Sasaki H, Nakano Y, Ino H (1991) Immunohistochemical examination of S-100 protein and substance P in the inner ear of the rat. Acta Otolaryngol Suppl 481:163–165. [PubMed: 1718135]

Jensen JB, Lysaght AC, Liberman MC, Qvortrup K, Stankovic KM (2015) Immediate and delayed cochlear neuropathy after noise exposure in pubescent mice. PLoS One 10:e0125160. [PubMed: 25955832]

Juhn SK (1988) Barrier systems in the inner ear. Acta Otolaryngol Suppl 458:79–83. [PubMed: 3245438]

Julander JG, Siddharthan V, Park AH, Preston E, Mathur P, Bertolio M, Wang H, Zukor K, Van Wettere AJ, Sinex DG, Morrey JD (2018) Consequences of in utero exposure to Zika virus in offspring of AG129 mice. Scientific reports 8:9384. [PubMed: 29925850]

Kastenbauer S, Klein M, Koedel U, Pfister HW (2001) Reactive nitrogen species contribute to blood-labyrinth barrier disruption in suppurative labyrinthitis complicating experimental pneumococcal meningitis in the rat. Brain Res 904:208–217. [PubMed: 11406118]

Keithley EM, Sharp P, Woolf NK, Harris JP (1988) Temporal sequence of viral antigen expression in the cochlea induced by cytomegalovirus. Acta Otolaryngol (Stockh) 106:46–54. [PubMed: 2844054]

Kikuchi T, Kimura RS, Paul DL, Adams JC (1995) Gap junctions in the rat cochlea: immunohistochemical and ultrastructural analysis. Anat Embryol (Berl) 191:101–118. [PubMed: 7726389]

Kimura RS (1969) Distribution, structure, and function of dark cells in the vestibular labyrinth. The Annals of otology, rhinology, and laryngology 78:542–561.

Kitajiri S, Miyamoto T, Mineharu A, Sonoda N, Furuse K, Hata M, Sasaki H, Mori Y, Kubota T, Ito J, Furuse M, Tsukita S (2004) Compartmentalization established by claudin-11-based tight junctions in stria vascularis is required for hearing through generation of endocochlear potential. J Cell Sci 117:5087–5096. [PubMed: 15456848]

Lang H, Ebihara Y, Schmiedt RA, Minamiguchi H, Zhou D, Smythe N, Liu L, Ogawa M, Schulte BA (2006) Contribution of bone marrow hematopoietic stem cells to adult mouse inner ear: mesenchymal cells and fibrocytes. The Journal of comparative neurology 496:187–201. [PubMed: 16538683]

Lazear HM, Govero J, Smith AM, Platt DJ, Fernandez E, Miner JJ, Diamond MS (2016) A Mouse Model of Zika Virus Pathogenesis. Cell Host Microbe 19:720–730. [PubMed: 27066744]

Leal MC, Muniz LF, Caldas Neto SD, van der Linden V, Ramos RC (2016a) Sensorineural hearing loss in a case of congenital Zika virus. Braz J Otorhinolaryngol.

Leal MC, Muniz LF, Ferreira TS, Santos CM, Almeida LC, Van Der Linden V, Ramos RC, Rodrigues LC, Neto SS (2016b) Hearing Loss in Infants with Microcephaly and Evidence of Congenital Zika Virus Infection - Brazil, November 2015-May 2016. MMWR Morb Mortal Wkly Rep 65:917–919. [PubMed: 27585248]

Li X, Shi X, Qiao Y, Xu K, Zeng L, Wang C, Xu Z, Niu H (2014) Observation of permeability of blood-labyrinth barrier during cytomegalovirus-induced hearing loss. Int J Pediatr Otorhinolaryngol 78:995–999. [PubMed: 24814236]

Likos A et al. (2016) Local Mosquito-Borne Transmission of Zika Virus - Miami-Dade and Broward Counties, Florida, June-August 2016. MMWR Morb Mortal Wkly Rep 65:1032–1038. [PubMed: 27684886]

Lindsay JR, Hemenway WG (1954) Inner ear pathology due to measles. The Annals of otology, rhinology, and laryngology 63:754–771.

Lindsay JR, Davey PR, Ward PH (1960) Inner ear pathology in deafness due to mumps. The Annals of otology, rhinology, and laryngology 69:918–935.

Liu F, Xia M, Xu A (2008) Expression of VEGF, iNOS, and eNOS is increased in cochlea of diabetic rat. Acta oto-laryngologica 128:1178–1186. [PubMed: 19241604]

Lopez IA, Ishiyama G, Lee M, Baloh RW, Ishiyama A (2007) Immunohistochemical localization of aquaporins in the human inner ear. Cell Tissue Res 328:453–460. [PubMed: 17318586]

Lowenstein O (1952) Recording of responses from individual end-organs of the vestibular apparatus. Proc R Soc Med 45:133–134. [PubMed: 14911875]

Mansuy JM, Dutertre M, Mengelle C, Fourcade C, Marchou B, Delobel P, Izopet J, Martin-Blondel G (2016) Zika virus: high infectious viral load in semen, a new sexually transmitted pathogen? Lancet Infect Dis 16:405.

Marcus DC, Shipley AM (1994) Potassium secretion by vestibular dark cell epithelium demonstrated by vibrating probe. Biophys J 66:1939–1942. [PubMed: 8075328]

Marcus DC, Shen Z (1994) Slowly activating voltage-dependent K+ conductance is apical pathway for K+ secretion in vestibular dark cells. Am J Physiol 267:C857–864. [PubMed: 7943212]

Marenholz I, Heizmann CW, Fritz G (2004) S100 proteins in mouse and man: from evolution to function and pathology (including an update of the nomenclature). Biochem Biophys Res Commun 322:1111–1122. [PubMed: 15336958]

Michetti F, D'Ambrosi N, Toesca A, Puglisi MA, Serrano A, Marchese E, Corvino V, Geloso MC (2019) The S100B story: from biomarker to active factor in neural injury. J Neurochem 148:168–187. [PubMed: 30144068]

Miyabe Y, Kikuchi T, Kobayashi T (2002) Comparative immunohistochemical localizations of aquaporin-1 and aquaporin-4 in the cochleae of three different species of rodents. Tohoku J Exp Med 196:247–257. [PubMed: 12086153]

Mounce BC, Poirier EZ, Passoni G, Simon-Loriere E, Cesaro T, Prot M, Stapleford KA, Moratorio G, Sakuntabhai A, Levraud JP, Vignuzzi M (2016) Interferon-Induced Spermidine-Spermine Acetyltransferase and Polyamine Depletion Restrict Zika and Chikungunya Viruses. Cell Host Microbe 20:167–177. [PubMed: 27427208]

Musso D, Roche C, Nhan TX, Robin E, Teissier A, Cao-Lormeau VM (2015a) Detection of Zika virus in saliva. Journal of clinical virology : the official publication of the Pan American Society for Clinical Virology 68:53–55. [PubMed: 26071336]

Musso D, Roche C, Robin E, Nhan T, Teissier A, Cao-Lormeau VM (2015b) Potential sexual transmission of Zika virus. Emerg Infect Dis 21:359–361. [PubMed: 25625872]

Nielsen S, Smith BL, Christensen EI, Agre P (1993) Distribution of the aquaporin CHIP in secretory and resorptive epithelia and capillary endothelia. Proc Natl Acad Sci U S A 90:7275–7279. [PubMed: 8346245]

O'Malley JT, Merchant SN, Burgess BJ, Jones DD, Adams JC (2009) Effects of fixative and embedding medium on morphology and immunostaining of the cochlea. Audiol Neurootol 14:78–87. [PubMed: 18827478]

Okano T, Nakagawa T, Kita T, Kada S, Yoshimoto M, Nakahata T, Ito J (2008) Bone marrow-derived cells expressing Iba1 are constitutively present as resident tissue macrophages in the mouse cochlea. J Neurosci Res 86:1758–1767. [PubMed: 18253944]

Okuda LS, Castilho G, Rocco DD, Nakandakare ER, Catanozi S, Passarelli M (2012) Advanced glycated albumin impairs HDL anti-inflammatory activity and primes macrophages for inflammatory response that reduces reverse cholesterol transport. Biochim Biophys Acta 1821:1485–1492. [PubMed: 22940078]

Pacher P, Beckman JS, Liaudet L (2007) Nitric oxide and peroxynitrite in health and disease. Physiological reviews 87:315–424. [PubMed: 17237348]

Paul AM, Shi Y, Acharya D, Douglas JR, Cooley A, Anderson JF, Huang F, Bai F (2014) Delivery of antiviral small interfering RNA with gold nanoparticles inhibits dengue virus infection in vitro. J Gen Virol 95:1712–1722. [PubMed: 24828333]

Popa R, Anniko M, Takumida M, Arnold W (2001) Localization of nitric oxide synthase isoforms in the human cochlea. Acta oto-laryngologica 121:454–459. [PubMed: 11508503]

Rasmussen SA, Jamieson DJ, Honein MA, Petersen LR (2016) Zika Virus and Birth Defects--Reviewing the Evidence for Causality. The New England journal of medicine 374:1981–1987. [PubMed: 27074377]

Rossi SL, Tesh RB, Azar SR, Muruato AE, Hanley KA, Auguste AJ, Langsjoen RM, Paessler S, Vasilakis N, Weaver SC (2016) Characterization of a Novel Murine Model to Study Zika Virus. Am J Trop Med Hyg 94:1362–1369. [PubMed: 27022155]

Rothermundt M, Peters M, Prehn JH, Arolt V (2003) S100B in brain damage and neurodegeneration. Microscopy research and technique 60:614–632. [PubMed: 12645009]

Sakaguchi N, Crouch JJ, Lytle C, Schulte BA (1998) Na-K-Cl cotransporter expression in the developing and senescent gerbil cochlea. Hearing research 118:114–122. [PubMed: 9606066]

Sato E, Shick HE, Ransohoff RM, Hirose K (2008) Repopulation of cochlear macrophages in murine hematopoietic progenitor cell chimeras: the role of CX3CR1. The Journal of comparative neurology 506:930–942. [PubMed: 18085589]

Schachtele SJ, Mutnal MB, Schleiss MR, Lokensgard JR (2011) Cytomegalovirus-induced sensorineural hearing loss with persistent cochlear inflammation in neonatal mice. J Neurovirol 17:201–211. [PubMed: 21416394]

Schraff SA, Schleiss MR, Brown DK, Meinzen-Derr J, Choi KY, Greinwald JH, Choo DI (2007) Macrophage inflammatory proteins in cytomegalovirus-related inner ear injury. Otolaryngol Head Neck Surg 137:612–618. [PubMed: 17903579]

Schulte B, Steel K (1994) Expression of alpha and beta subunit isoforms of Na,K-ATPase in the mouse inner ear and changes with mutations at the Wv or Sld loci. Hearing research 78:65–76. [PubMed: 7961179]

Schulte BA, Adams JC (1989) Distribution of immunoreactive Na+,K+-ATPase in gerbil cochlea. J Histochem Cytochem 37:127–134. [PubMed: 2536055]

Shapiro-Mendoza CK et al. (2017) Pregnancy Outcomes After Maternal Zika Virus Infection During Pregnancy - U.S. Territories, January 1, 2016-April 25, 2017. MMWR Morb Mortal Wkly Rep 66:615–621. [PubMed: 28617773]

Shi SR, Tandon AK, Cote C, Kalra KL (1992) S-100 protein in human inner ear: use of a novel immunohistochemical technique on routinely processed, celloidin-embedded human temporal bone sections. Laryngoscope 102:734–738. [PubMed: 1614244]

Spicer S, Schulte B (1991) Differentiation of inner ear fibrocytes according to their ion transport related activity. Hearing research 56:53–64. [PubMed: 1663106]

Stankovic KM, Adams JC, Brown D (1995) Immunolocalization of aquaporin CHIP in the guinea pig inner ear. Am J Physiol 269:C1450–1456. [PubMed: 8572173]

Steiner J, Bernstein HG, Bogerts B, Gos T, Richter-Landsberg C, Wunderlich MT, Keilhoff G (2008) S100B is expressed in, and released from, OLN-93 oligodendrocytes: Influence of serum and glucose deprivation. Neuroscience 154:496–503. [PubMed: 18472341]

Takumida M, Anniko M (2001a) Direct evidence of nitric oxide production in the guinea pig organ of Corti. Acta oto-laryngologica 121:342–345. [PubMed: 11425198]

Takumida M, Anniko M (2001b) Detection of nitric oxide in the guinea pig inner ear, using a combination of aldehyde fixative and 4,5-diaminofluorescein diacetate. Acta oto-laryngologica 121:460–464. [PubMed: 11508504]

Takumida M, Anniko M (2002) Nitric oxide in the inner ear. Current opinion in neurology 15:11–15. [PubMed: 11796945]

Takumida M, Anniko M (2004) Functional significance of nitric oxide in the inner ear. In Vivo 18:345–350. [PubMed: 15341190]

Takumida M, Kakigi A, Egami N, Nishioka R, Anniko M (2012) Localization of aquaporins 1, 2, and 3 and vasopressin type 2 receptor in the mouse inner ear. Acta oto-laryngologica 132:807–813. [PubMed: 22768909]

Tan Z, Zhang W, Sun J, Fu Z, Ke X, Zheng C, Zhang Y, Li P, Liu Y, Hu Q, Wang H, Zheng Z (2018) ZIKV infection activates the IRE1-XBP1 and ATF6 pathways of unfolded protein response in neural cells. J Neuroinflammation 15:275. [PubMed: 30241539]

Tornabene SV, Sato K, Pham L, Billings P, Keithley EM (2006) Immune cell recruitment following acoustic trauma. Hearing research 222:115–124. [PubMed: 17081714]

Uraki R, Hwang J, Jurado KA, Householder S, Yockey LJ, Hastings AK, Homer RJ, Iwasaki A, Fikrig E (2017) Zika virus causes testicular atrophy. Sci Adv 3:e1602899. [PubMed: 28261663]

Valdespino-Vazquez MY, Sevilla-Reyes EE, Lira R, Yocupicio-Monroy M, Piten-Isidro E, Boukadida C, Hernandez-Pando R, Soriano-Jimenez JD, Herrera-Salazar A, Figueroa-Damian R, Reyes-Teran G, Zamora-Escudero R, Cardona-Perez JA, Maldonado-Rodriguez A, Moreno-Verduzco ER, Torres-Flores JM (2019) Congenital Zika Syndrome and Extra-Central Nervous System Detection of Zika Virus in a Pre-term Newborn in Mexico. Clin Infect Dis 68:903–912. [PubMed: 30188990]

Vetter DE, Mann JR, Wangemann P, Liu J, McLaughlin KJ, Lesage F, Marcus DC, Lazdunski M, Heinemann SF, Barhanin J (1996) Inner ear defects induced by null mutation of the isk gene. Neuron 17:1251–1264. [PubMed: 8982171]

Vinhaes ES, Santos LA, Dias L, Andrade NA, Bezerra VH, de Carvalho AT, de Moraes L, Henriques DF, Azar SR, Vasilakis N, Ko AI, Andrade BB, Siqueira IC, Khouri R, Boaventura VS (2017) Transient Hearing Loss in Adults Associated With Zika Virus Infection. Clin Infect Dis 64:675–677. [PubMed: 27927858]

Von Bekesy G (1952) Resting potentials inside the cochlear partition of the guinea pig. Nature 169:241–242. [PubMed: 14910737]

Wang H, Zhang L, Zhang IY, Chen X, Da Fonseca A, Wu S, Ren H, Badie S, Sadeghi S, Ouyang M, Warden CD, Badie B (2013) S100B promotes glioma growth through chemoattraction of myeloid-derived macrophages. Clin Cancer Res 19:3764–3775. [PubMed: 23719262]

Wang Y, Ren C (2012) Effects of repeated “benign” noise exposures in young CBA mice: shedding light on age-related hearing loss. J Assoc Res Otolaryngol 13:505–515. [PubMed: 22532192]

Xia A, Kikuchi T, Hozawa K, Katori Y, Takasaka T (1999) Expression of connexin 26 and Na,K-ATPase in the developing mouse cochlear lateral wall: functional implications. Brain Res 846:106–111. [PubMed: 10536217]

Xia A, Katori Y, Oshima T, Watanabe K, Kikuchi T, Ikeda K (2001) Expression of connexin 30 in the developing mouse cochlea. Brain Res 898:364–367. [PubMed: 11306024]

Xia AP, Ikeda K, Katori Y, Oshima T, Kikuchi T, Takasaka T (2000) Expression of connexin 31 in the developing mouse cochlea. Neuroreport 11:2449–2453. [PubMed: 10943702]

Xia JH, Liu CY, Tang BS, Pan Q, Huang L, Dai HP, Zhang BR, Xie W, Hu DX, Zheng D, Shi XL, Wang DA, Xia K, Yu KP, Liao XD, Feng Y, Yang YF, Xiao JY, Xie DH, Huang JZ (1998) Mutations in the gene encoding gap junction protein beta-3 associated with autosomal dominant hearing impairment. Nat Genet 20:370–373. [PubMed: 9843210]

Yamane H, Takayama M, Konishi K, Iguchi H, Shibata S, Sunami K, Nakai Y (1997) Nitric oxide synthase and contractile protein in the rat cochlear lateral wall: possible role of nitric oxide in regulation of strial blood flow. Hearing research 108:65–73. [PubMed: 9213123]

Yang W, Vethanayagam RR, Dong Y, Cai Q, Hu BH (2015) Activation of the antigen presentation function of mononuclear phagocyte populations associated with the basilar membrane of the cochlea after acoustic overstimulation. Neuroscience 303:1–15. [PubMed: 26102003]

Highlights:

- Postnatal Zika virus damages inner ear end organs.
- Cochlear and vestibular hair cells are compromised by Zika virus infection.
- Endolymph production systems are damaged by Zika virus infection.
- Zika virus infection up-regulates damage-associated molecular pattern molecules.
- Zika virus infection damages spiral ganglion neurons.

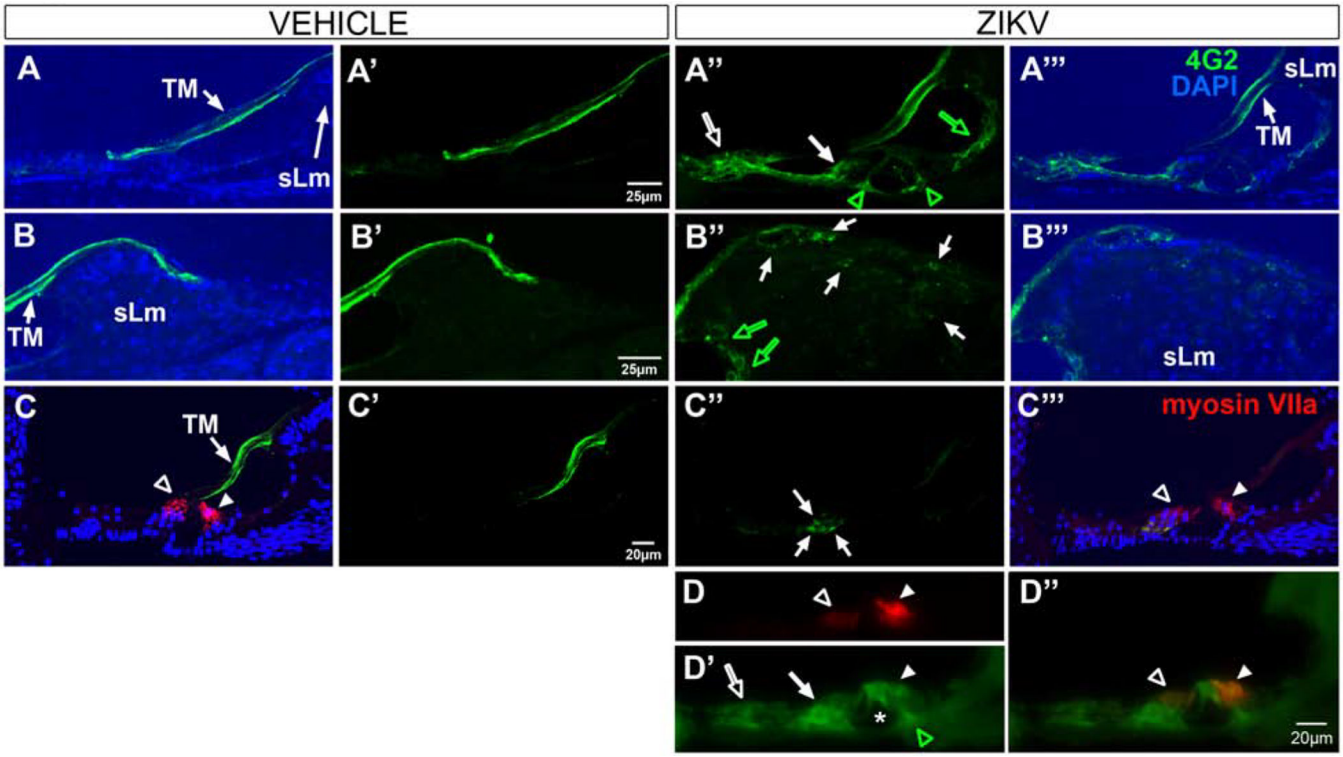

Figure 1.

4G2 protein is localized in the cochlear epithelium and spiral limbus in *Ifnar1*$^{-/-}$ ZIKV infected mice. 4G2 is not detected in the cochlear epithelium or spiral limbus of vehicle-treated mice (A-C, A'-C'). Capricious non-specific staining of the tectorial membrane (TM) is detected in vehicle and ZIKV-infected cases. In ZIKV infected mice, 4G2 is localized in pillar cells (green open arrowheads, A", D'), medial (green open arrow, A"; green open arrows, B") and lateral support cells (white open arrow, A", D'), Deiter's cells (closed arrow, A", C", D') and an inner hair cell (closed arrowhead, D', D"). Myosin VIIa staining shows hair cell labeling (arrowheads, C"', D). No double labeled support cells (e.g. Deiter's cells) are detected (c.f. C", C"') but a double labeled inner hair cell is shown (closed arrowhead, D"). 4G2 is also localized to fibrocytes in the spiral limbus (sLm, white arrows, B"). DAPI counterstains are shown (A-C, A"'-C"'). Scale bar for A-A"' in A'. Scale bar for B-B"' in B'. Scale bar for C-C"' in C'. Scale bar for D and D' in D".

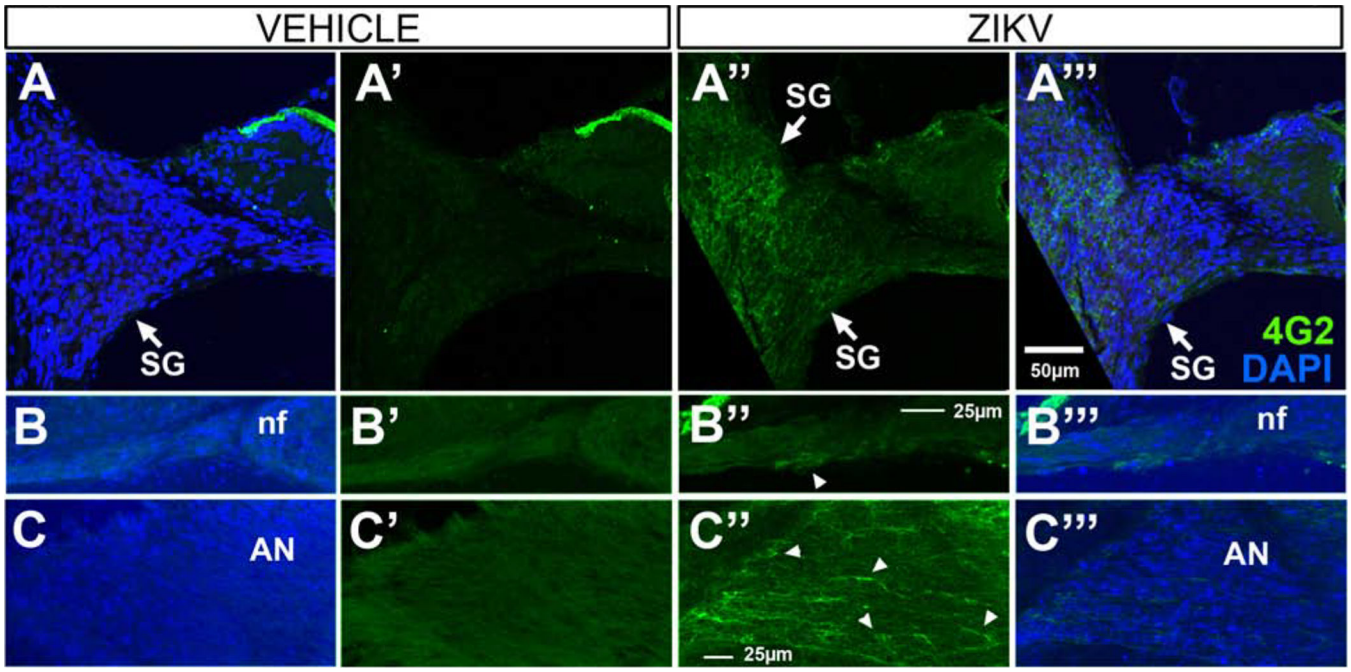

Figure 2.

4G2 protein is localized in spiral ganglion neurons, nerve fibers and the auditory nerve in *Ifnar1*$^{-/-}$ ZIKV infected mice. 4G2 is localized in spiral ganglion (SG) neurons (A"), at a low level within the nerve fiber (nf) region traversed by spiral ganglion dendrites and olivocochlear efferents beneath the cochlear epithelium (arrowhead, B") and within the auditory nerve (AN; arrowheads indicate examples of immunopositive fibers, C") in ZIKV infected mice. 4G2 is not detected in spiral ganglion neurons, nerve fibers or the auditory nerve of vehicle-treated mice (A-C, A'-C'). DAPI counterstains are shown (A-C, A"'-C"'). Scale bar for A - A" in A"', scale bar for B-B"' in B" and scale bar for C-C"' in C".

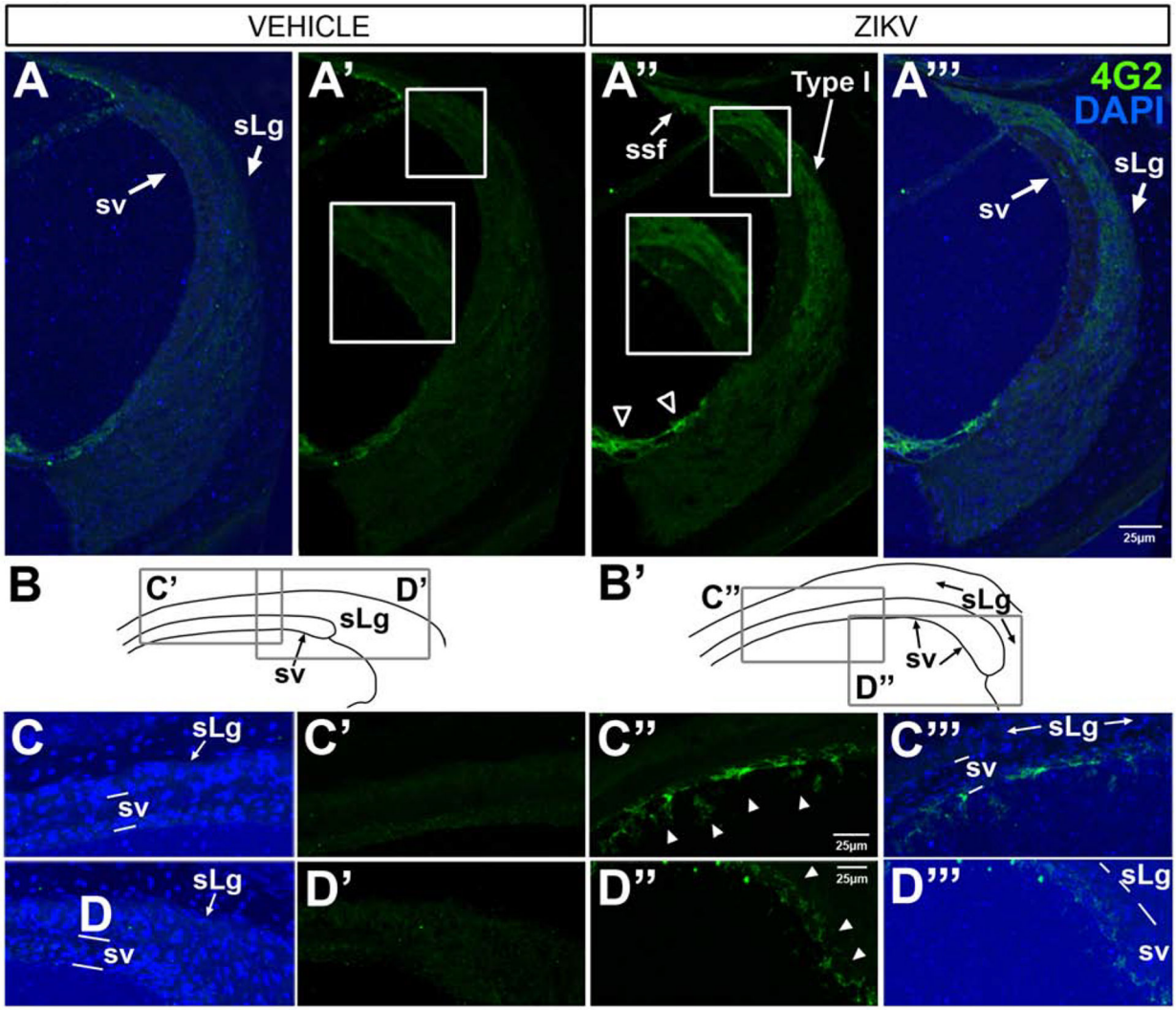

Figure 3.

4G2 protein is localized in the lateral wall of the cochlea in *Ifnar1*$^{-/-}$ ZIKV infected mice. Through the midturn of the cochlea, 4G2 is not seen in the spiral ligament or stria vascularis in vehicle-treated cases (A'; DAPI-counterstained, A), but 4G2 is localized in the lateral support cells (open arrowheads in A", A"'), the spiral ligament (sLg), suprastrial (ssf) and Type I fibrocytes (A", A"') and cells within the laminae of the stria vascularis (A", A"') after ZIKV infection. The small boxed regions (A' and A") showing regions of higher magnification views in the larger boxes (A and A") reveal 4G2 localization in the stria vascularis and spiral ligament after ZIKV infection (A") and not after vehicle injection (A'). The apical turn of the cochlea contains 4G2-positive cells (arrowheads C", D", C"', D"') with different cellular morphologies dependent on location. Line drawing schematics of vehicle controls (B) and ZIKV infected (B') indicate regions shown at higher magnification C-D"'). DAPI counterstains are shown (A, C, D, A"', C"',D"'). Scale bar for A - A" in A"', scale bar for C, C' and C"' in C" and scale bar for D. D' and D"' in D".

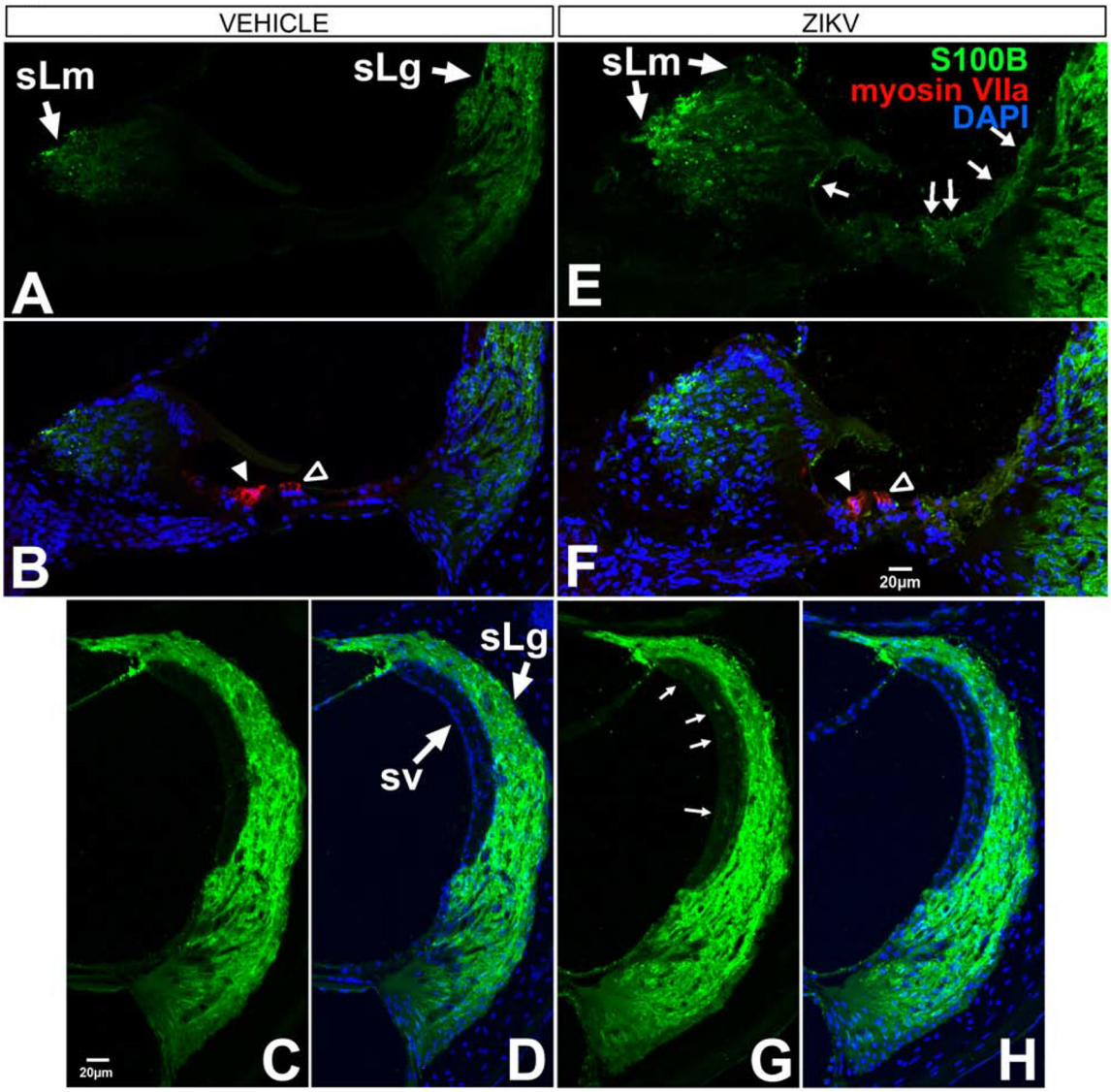

Figure 4.

S100B is localized in the cochlear epithelium, spiral limbus and lateral wall of the cochlea in *Ifnar1*$^{-/-}$ ZIKV infected mice. Baseline S100B localization is found in the spiral limbus (sLm, A, B), spiral ligament (sLg, A-D) and no localization in the cochlear epithelium (A, B) in vehicle-treated mice. S100B is upregulated in the cochlear epithelium (arrows in E; F), spiral limbus (sLm, E, F) and intermediate layer of the stria vascularis (sv; arrows in G; H) following ZIKV infection. Myosin VIIa staining of inner (closed arrowhead B and F) and outer (open arrowhead B and F) shows no co-labeling with S100B (F). DAPI counterstains are shown (B, D, F, H). Scale bar for A B, E in F. Scale bar for D, G, H in C.

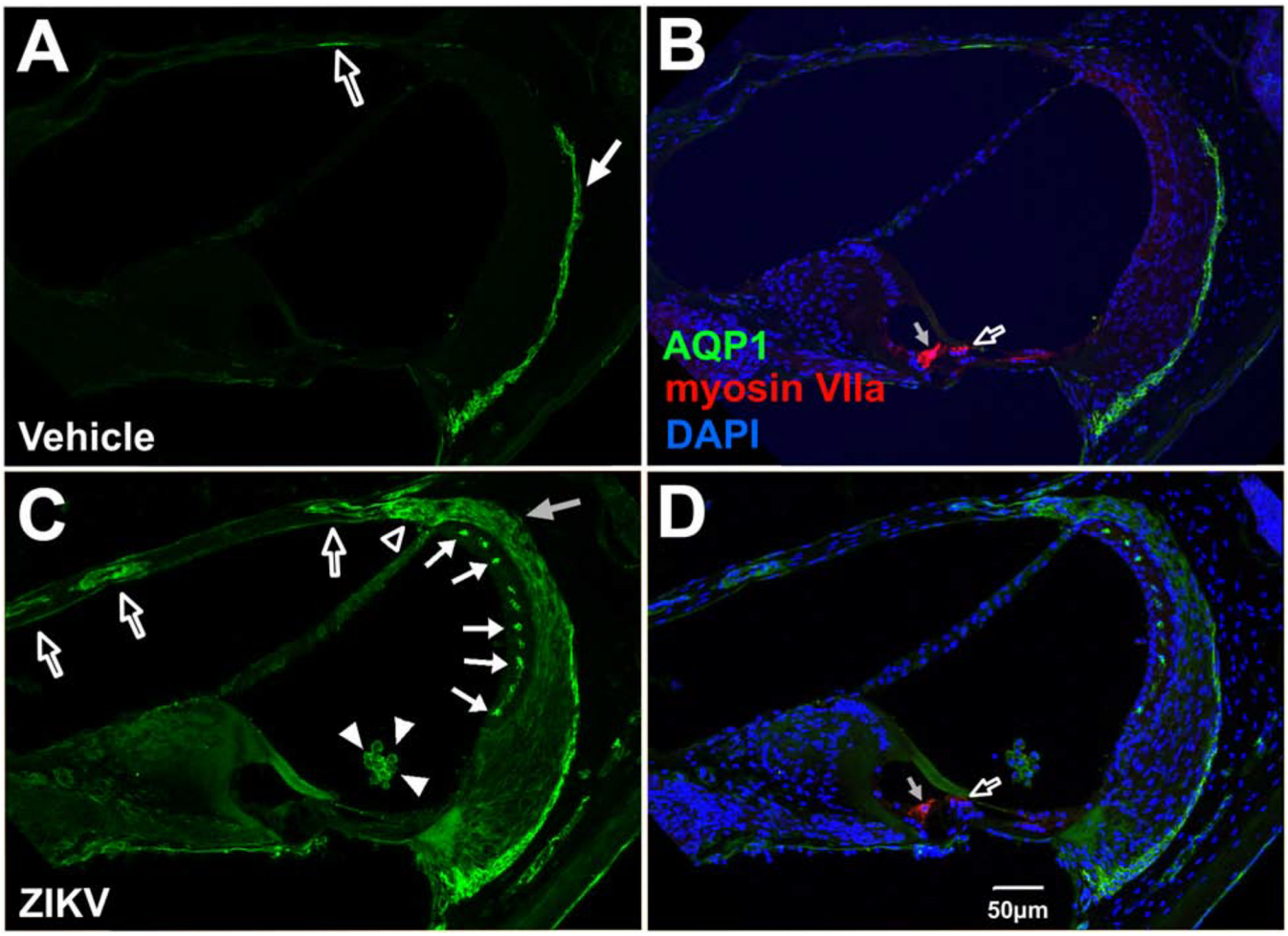

Figure 5.

Aquaporin-1 localization in the cochlea, scala media and lateral wall of the cochlea in *Ifnar1*$^{-/-}$ ZIKV infected mice. Vehicle-injected mice show baseline AQP1 localization in type III fibrocytes of the spiral ligament (arrow in A; B) and a low level of protein localization in the endosteum of the scala vestibuli (open arrow in A; B). Postnatal ZKV infection shows upregulation of AQP1 in suprastrial fibrocytes (open arrowhead, C), Type I fibrocytes in the spiral ligament (gray arrow, C), the intermediate region of the stria vascularis (closed arrows, D) and in structures with a vascular appearance in the osseous spiral lamina above the scala vestibuli (open arrows, C). AQP1 is also localized to cells in the scala media (closed arrowheads in C; D) whose nuclei are stained with DAPI (D). Myosin VIIa of inner (gray arrow, B and D) and outer (open arrow, B and D) hairs cells are not double labeled with AQP1 with vehicle treatment (B) or ZIKV infection (D). DAPI counterstains are shown (B, D). Scale bar for A-C in D.

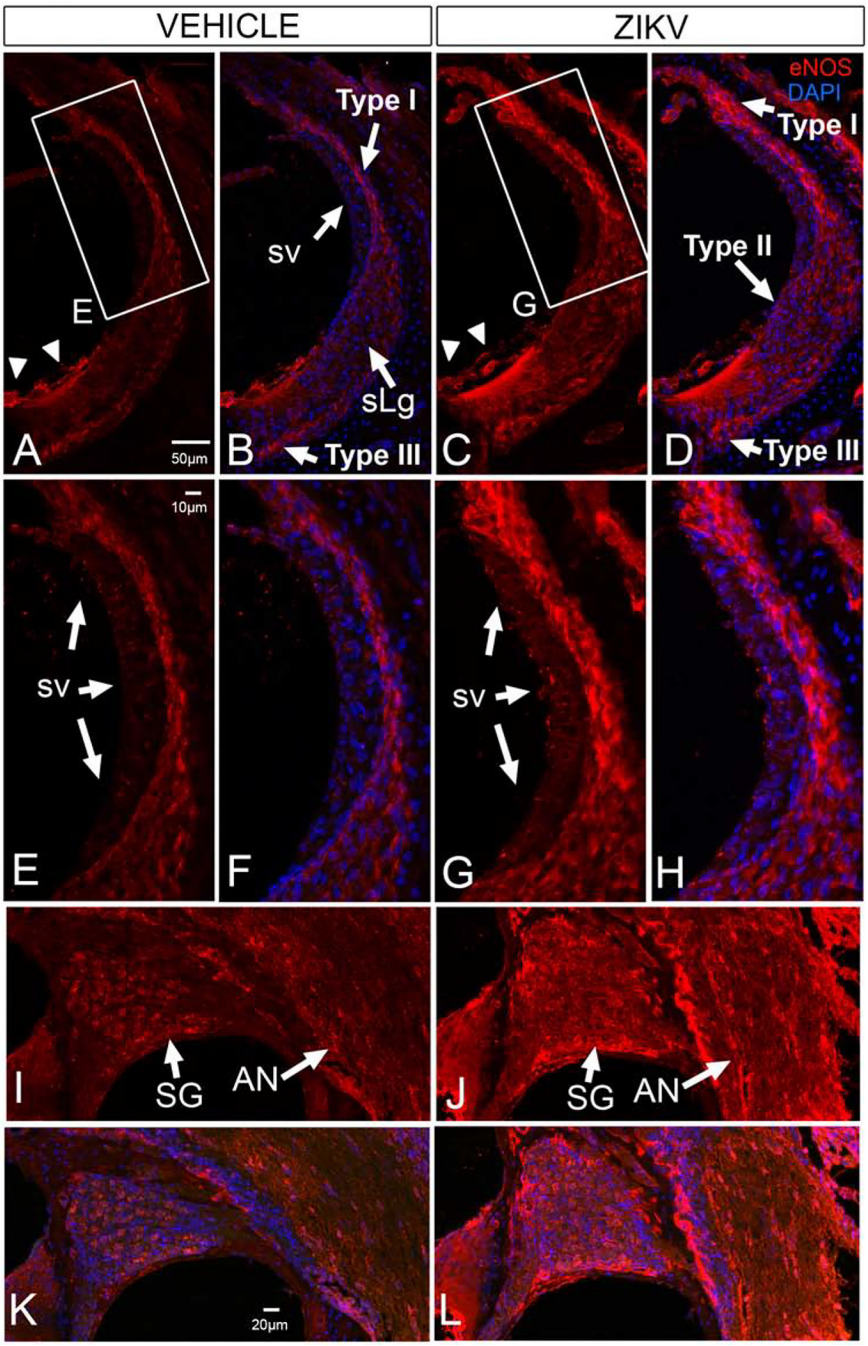

Figure 6.

eNOS is upregulated the cochlear lateral wall, spiral ganglion and auditory nerve of *Ifnar1*$^{-/-}$ ZIKV infected mice. Baseline eNOS localization is seen in Type I and Type III fibrocytes of the spiral ligament (sLg, A, B, E, F), stria vascularis (sv, A, B, E, F), in lateral support cells (arrowheads in A; B), neurons of the spiral ganglion (SG, I, K) and the auditory nerve (AN, I, K) in vehicle injected mice. ZKV infection shows upregulation of eNOS in the Type I, Type II and Type III fibrocytes in the spiral ligament and stria vascularis (C, D, G, H) where immunoreactivity appears as larger aggregates. eNOS is also upregulated

in spiral ganglion neurons in a nonneuronal pattern and in the auditory nerve (J, L). eNOS is not upregulated in the cochlear epithelium after ZIKV infection (cf C, D to A, B). DAPI counterstains are shown (B, D, F, H, K, L). Boxed regions in A and C shown in E and G, respectively. Scale bar for B-D in A. Scale bar for F-H in E. Scale bar for I-L in K.

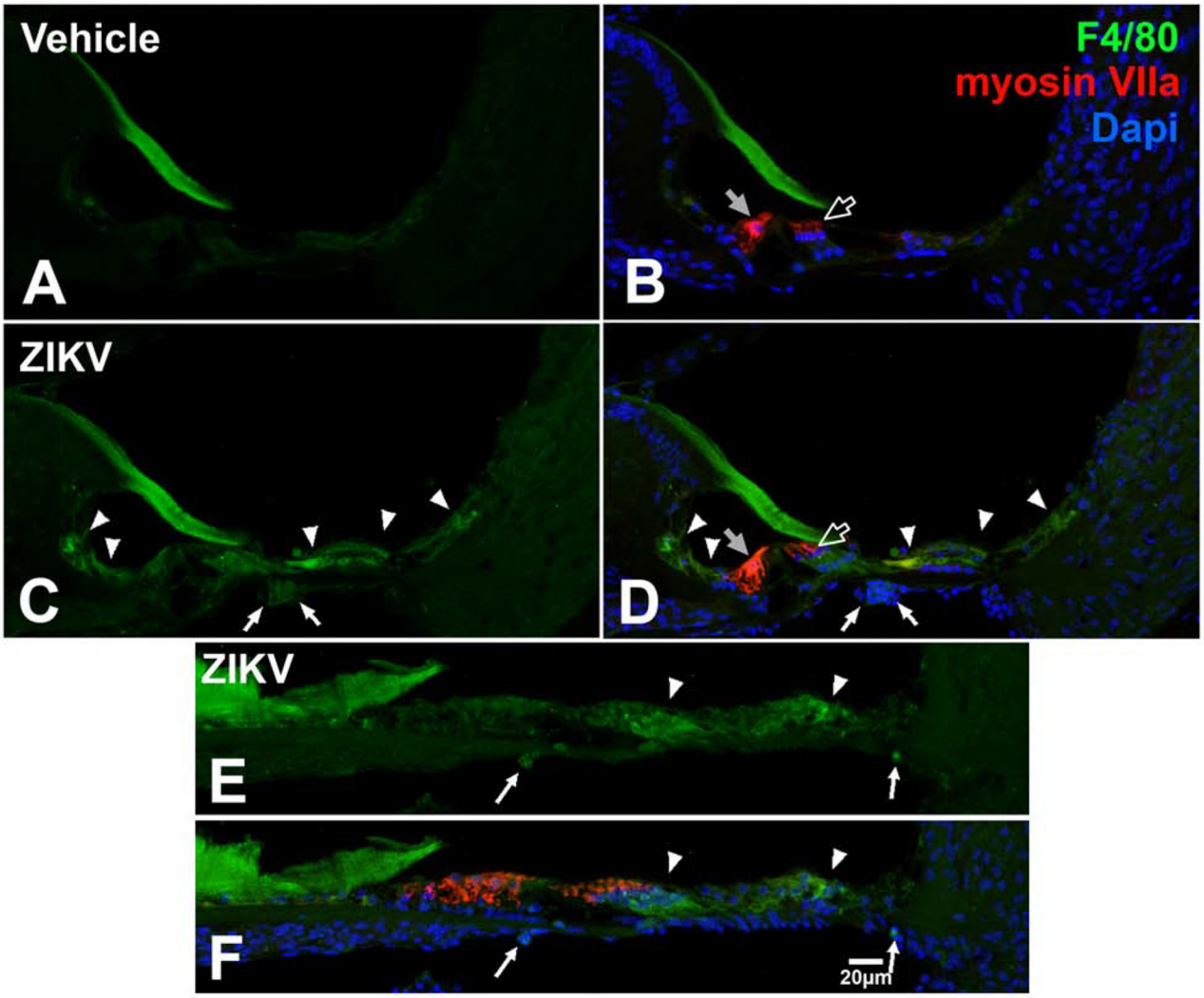

Figure 7.

F4/80 is localized in the cochlea in *Ifnar1*$^{-/-}$ ZIKV infected mice. F4/80 is not localized in the cochlea in vehicle-treated mice (A, B). F4/80 is upregulated in the cochlear epithelium (arrowheads C, D) and in cells beneath the basilar membrane (arrows; C, D, E, F) following ZIKV infection. Myosin VIIa staining of inner (gray arrow, B and D) and outer (open arrow, B and D) shows that hairs cells are not double labeled with F4/80 following vehicle treatment (B) or ZIKV infection (D). The gelatinous matrix of the tectorial membrane shows non-specific labeling (A-D). DAPI counterstains are shown (B, D, F). Scale bar for A-E in F.

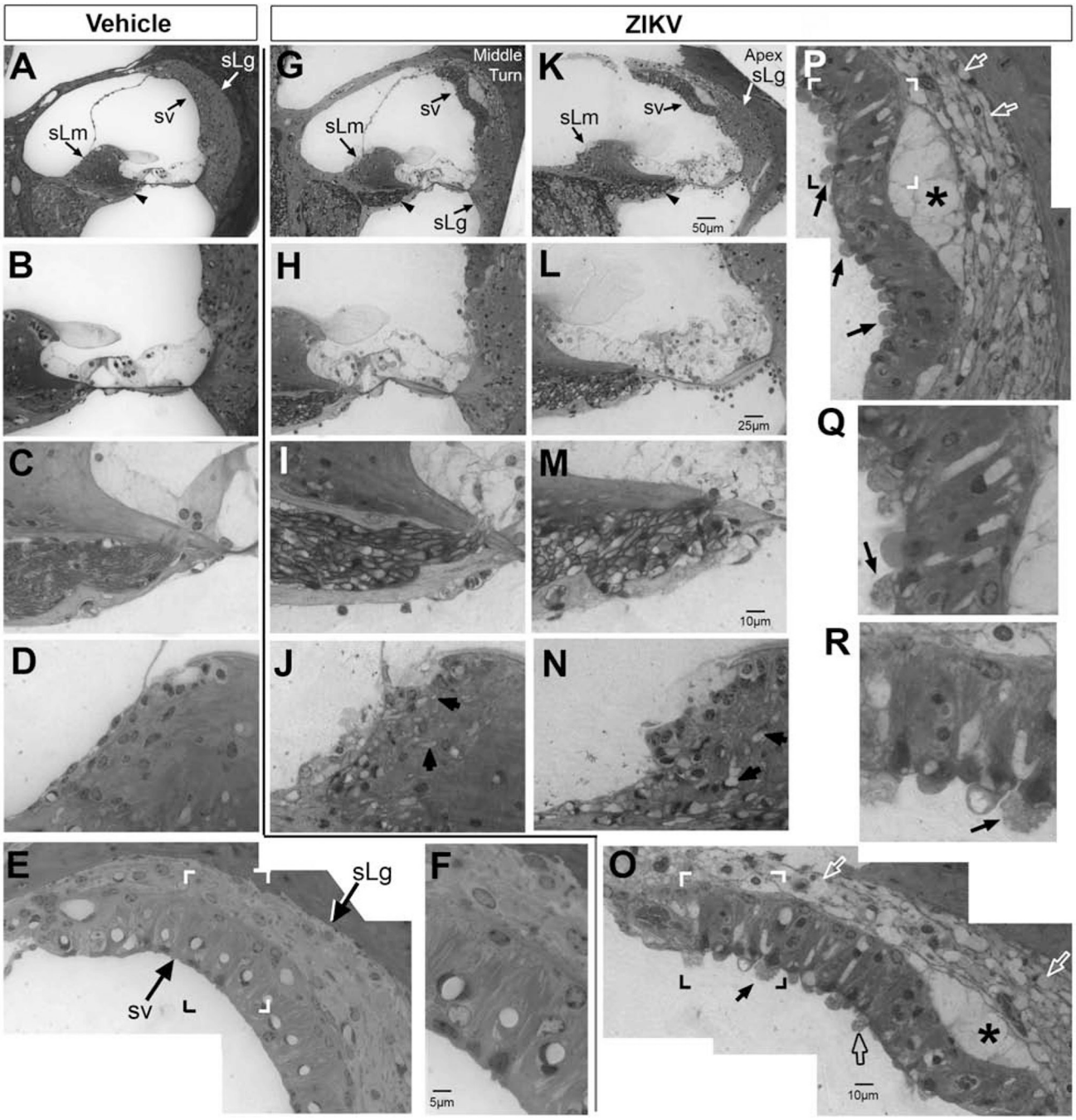

Figure 8.

Postnatal ZIKV infection of *Ifnar1*$^{-/-}$ mice causes damage to the cochlea. The cochlear epithelium (A. B), spiral limbus (sLm, A, D) and stria vascularis (sv, A, E, F) of vehicle-treated mice appear morphologically normal. Nerve fibers (arrowhead in A; C) beneath the spiral limbus have normal small diameter profiles. In ZIKV infected mice, the cochlear epithelium exhibits damage in the middle turn (G, H) and damage appears more severe at the apex (K, L). After ZIKV infection, the spiral ligament (sLg, G, K, O, P) and stria vascularis (sv, G, K, O, P, enlarged insets are shown in Q and R) also show evidence of damage. Spiral

ligament fibrocytes have a vacuolated appearance (white open arrows; O and P) and regions of the lateral wall show a loss of continuity between the stria vascularis and spiral ligament (G, K, asterisks in P and O). Regions of the apical surface of the stria vascularis form protrusions of cytoplasm containing vesicles/vacuoles (open black arrow O; P). Evidence of release of vacuoles was seen (data not shown). In some cases, the nucleus was translocated to the apical surface, possibly in preparation for expulsion of the cell from the epithelium (examples shown, closed black arrows; O, P, Q, R). Nerve fibers beneath the spiral limbus in the middle turn have large diameter profiles (I); at the apex, nerve fibers and their myelinated sheaths were swollen to a greater extent (M) than the middle turn. Scale bar for A and G in K. Scale bar for B and H in L. Scale bar for C, D, I, J, N in M. Scale bar for E and P in O. Scale bar for Q and R in F.

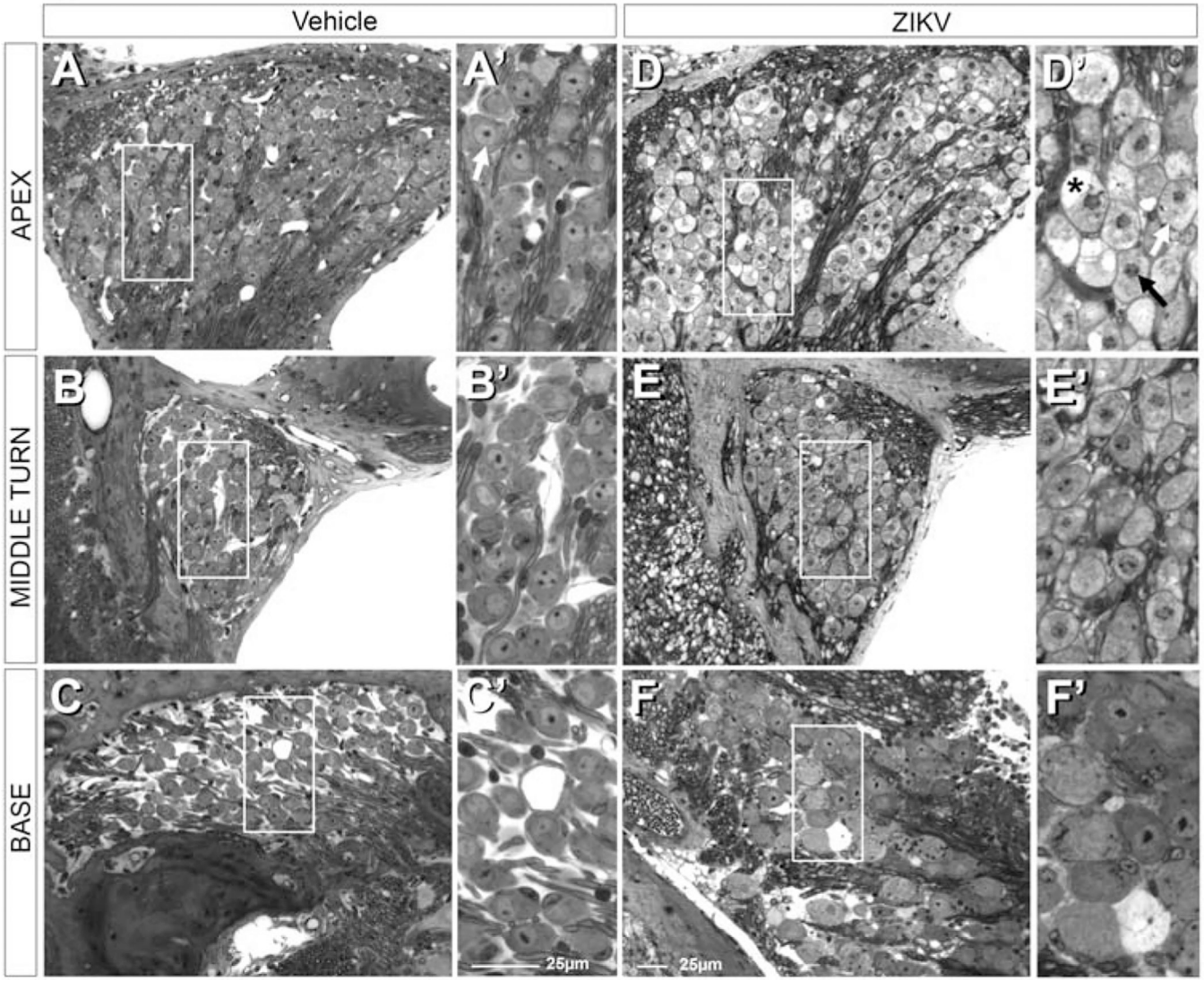

Figure 9.

Postnatal ZIKV infection of *Ifnar1*$^{-/-}$ mice produces graded damage in spiral ganglion neurons (boxed regions in A-C indicate regions shown at higher magnification in A'-C', respectively). Following postnatal vehicle treatment, immune compromised mice maintain normal neuronal morphology of spiral ganglion neurons throughout the cochlear spiral (A-C). This includes normal cytoplasm and nuclei with prominent nucleoli (white arrow, A'). Postnatal ZIKV infection results in apparently swollen axons and fibers in the auditory nerve and surrounding the spiral ganglion neurons (D-F). Boxed regions in D-F shown at higher magnification in D'-F', respectively. Spiral ganglion neurons at the apex (D and D') have mottled cytoplasm (white arrow), vacuoles (asterisk) and condensed nuclei (black arrow, D'); nucleoli were not readily detectable. In the middle turn of the cochlea, fewer spiral ganglion neurons have mottled cytoplasm (E and E'). Even fewer spiral ganglion neurons with mottled cytoplasm are seen at the base of the cochlea (F and F'). While rare, some ganglion cell degeneration is still observed in basal turns (F'). Some spiral ganglion neurons at the base of the cochlea show relatively normal neuronal morphology with euchromatic

nuclei, prominent nucleoli and uniformly stained cytoplasm, but are larger in size than vehicle treated spiral ganglion neurons at the base of the cochlea (cf. F to C and F’ to C’).

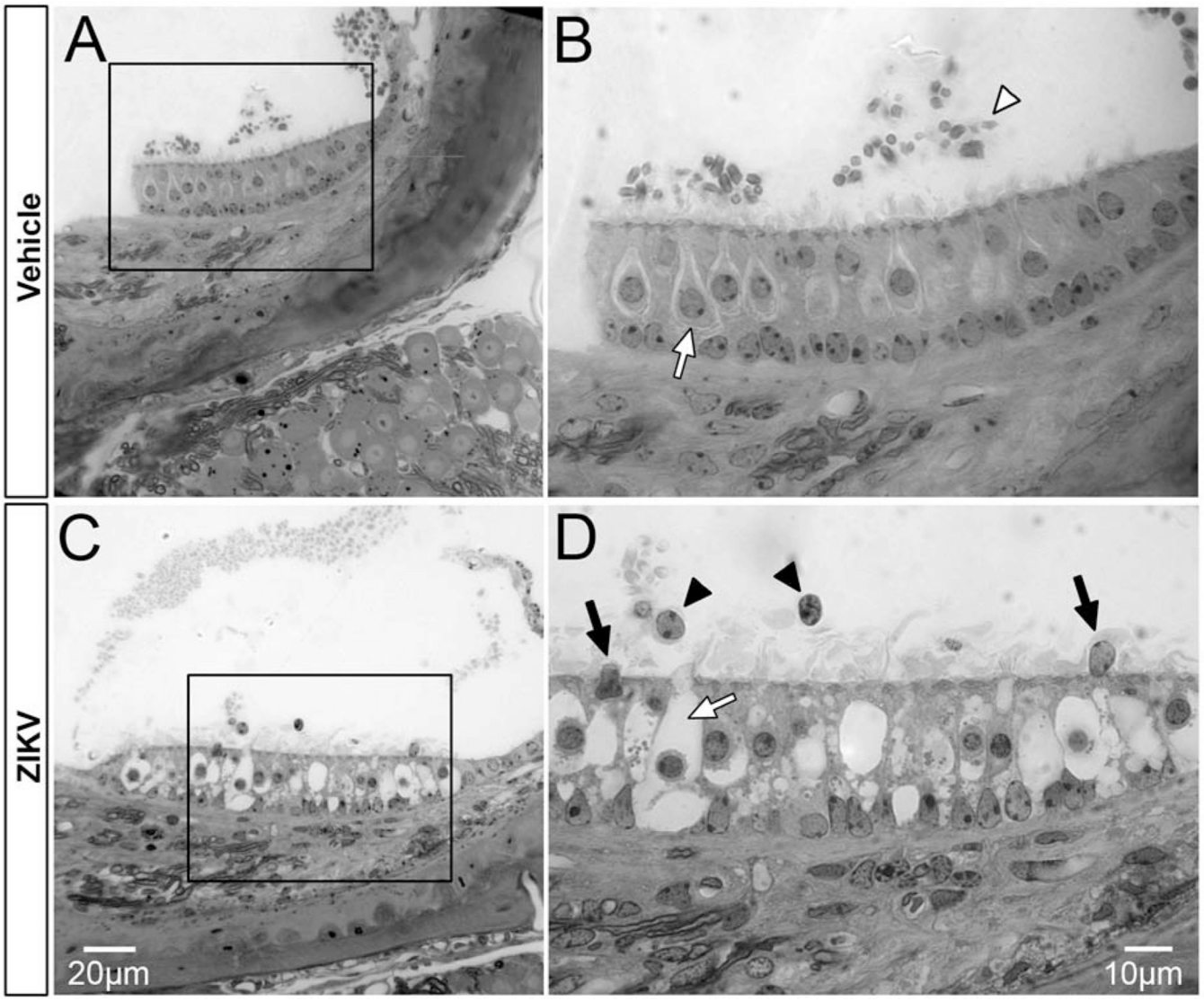

Figure 10.

Postnatal ZIKV infection of *Ifnar1*$^{-/-}$ mice damages the saccular macula. The epithelium of the saccular macula exhibits normal integrity following vehicle injection (A, boxed region in A is shown in B). Otoconia are present above the macula (A; white arrowhead, B) and hair cells with normal morphology are present in the epithlium (white arrow, Type I hair cell and surrounding afferent calyx). After ZIKV infection, vacuolation is seen in the epithelium of the saccular macula (C; high magnification of C is shown in D). Large flask shaped spaces maintaining continuity to the apical surface are presumed to have been occupied by hair cells and their stereocilia (white arrow, D). Nuclei are seen in the endolymph above the epithelium of the saccular macula (black arrowheads, D) and may have been extruded from the epithelium as two nuclei located at the epithelial surface are likely to be in the process of extrusion (black arrows, D). Scale bar for A in C, scale bar for B in D.

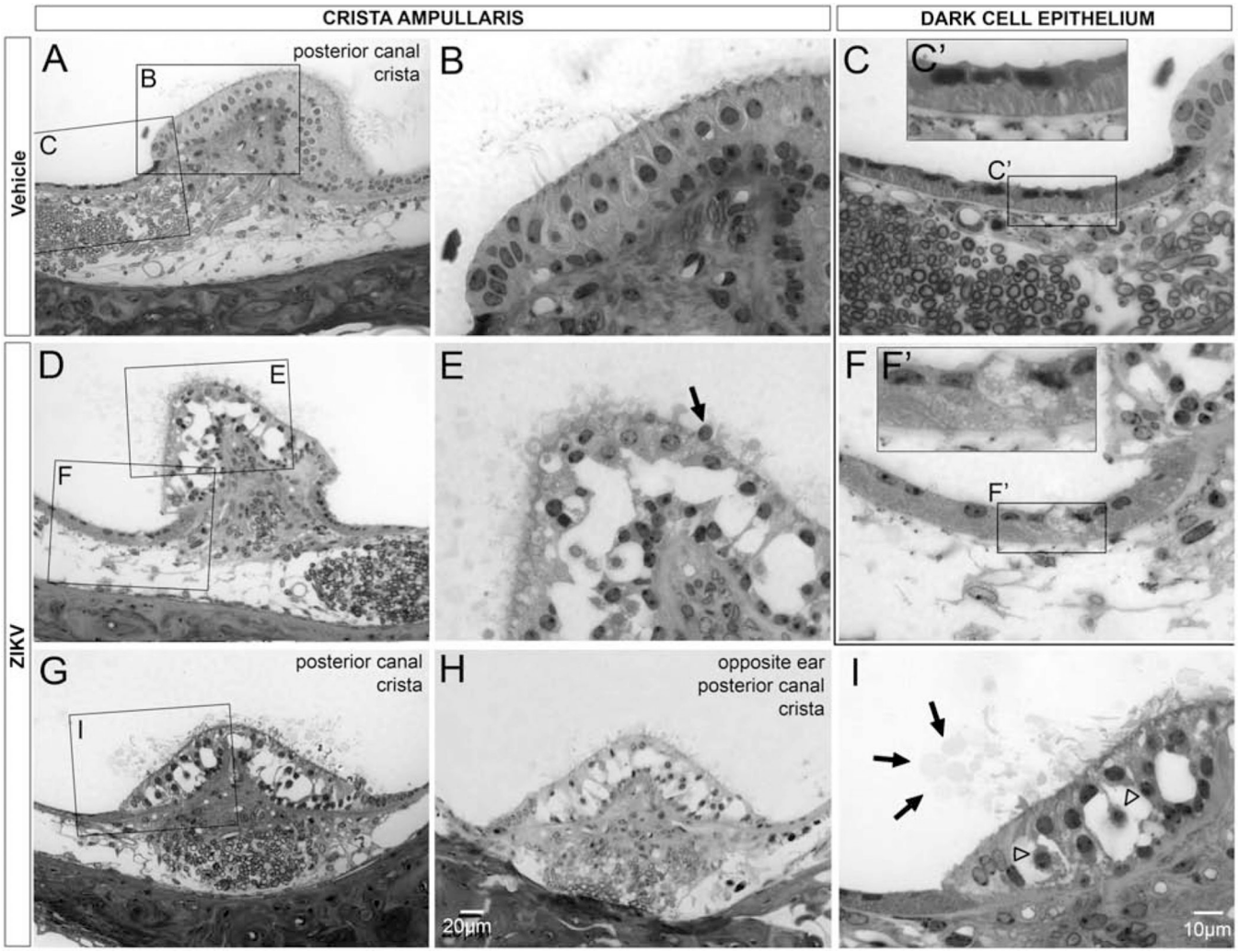

Figure 11.

Postnatal ZIKV infection of *Ifnar1*$^{-/-}$ mice causes damage to the epithelium of the crista ampullaris. The epithelium of the posterior canal crista shows normal integrity, with neighboring cells closely apposed, in vehicle treated mice (A, B). Vacuolation of the posterior canal crista epithelium is seen after ZKV infection (D, G, H; higher magnification E, I). Vacuolization the posterior canal crista occurs bilaterally (G, H). Cell shrinkage (open arrowheads, I), nuclear extrusion (arrow, E) and presence of vesicles above the apical surface of the crista epithelium (arrows, I) were all observed in the region of the crista ampullaris in ZIKV infected mice. The dark cell associated epithelium reveals normal integrity with striations beneath the apically located nuclei in vehicle-treated mice (C, C'). In ZIKV infected mice, the epithelium associated with the dark cells contain numerous vesicles that obliterate the normal striations and there is also loss of integrity of the apical surface (F, F'). Insets show higher magnification views of the dark cell epithelium (C', F'). Scale bar for A, D, G, in H. Scale bar for B, C, E, F, in I.